Published in final edited form as:

Cell Rep. 2024 August 27; 43(8): 114495. doi:10.1016/j.celrep.2024.114495.

Movement-related increases in subthalamic activity optimize locomotion

Joshua W. Callahan[1], **Juan Carlos Morales**[1], **Jeremy F. Atherton**[1], **Dorothy Wang**[1], **Selena Kostic**[1], **Mark D. Bevan**[1,2,*]

[1]Department of Neuroscience, Feinberg School of Medicine, Northwestern University, Chicago, IL 60611, USA

[2]Lead contact

Abstract

The subthalamic nucleus (STN) is traditionally thought to restrict movement. Lesion or prolonged STN inhibition increases movement vigor and propensity, while optogenetic excitation has opposing effects. However, STN neurons often exhibit movement-related increases in firing. To address this paradox, STN activity was recorded and manipulated in head-fixed mice at rest and during self-initiated and self-paced treadmill locomotion. We found that (1) most STN neurons (type 1) exhibit locomotion-dependent increases in activity, with half firing preferentially during the propulsive phase of the contralateral locomotor cycle; (2) a minority of STN neurons exhibit dips in activity or are uncorrelated with movement; (3) brief optogenetic inhibition of the lateral STN (where type 1 neurons are concentrated) slows and prematurely terminates locomotion; and (4) in Q175 Huntington's disease mice, abnormally brief, low-velocity locomotion is associated with type 1 hypoactivity. Together, these data argue that movement-related increases in STN activity contribute to optimal locomotor performance.

Graphical Abstract

*Correspondence: m-bevan@northwestern.edu.

AUTHOR CONTRIBUTIONS

Conceptualization: J.W.C. and M.D.B.; methodology: J.W.C., J.C.M., J.F.A., and M.D.B.; validation: J.W.C., J.C.M., J.F.A., and M.D.B.; formal analysis: J.W.C., J.C.M., J.F.A., and M.D.B.; investigation: J.W.C., D.W., and S.K.; data curation: J.W.C. and M.D.B.; writing – original draft, J.W.C. and M.D.B.; writing – editing, J.W.C., J.C.M., J.F.A., D.W., S.K., and M.D.B.; visualization, J.W.C., J.C.M., J.F.A., and M.D.B.; supervision, J.W.C. and M.D.B.; project administration, J.W.C. and M.D.B.; funding acquisition, M.D.B.

DECLARATION OF INTERESTS

The authors declare no competing interests.

SUPPLEMENTAL INFORMATION

Supplemental information can be found online at https://doi.org/10.1016/j.celrep.2024.114495.

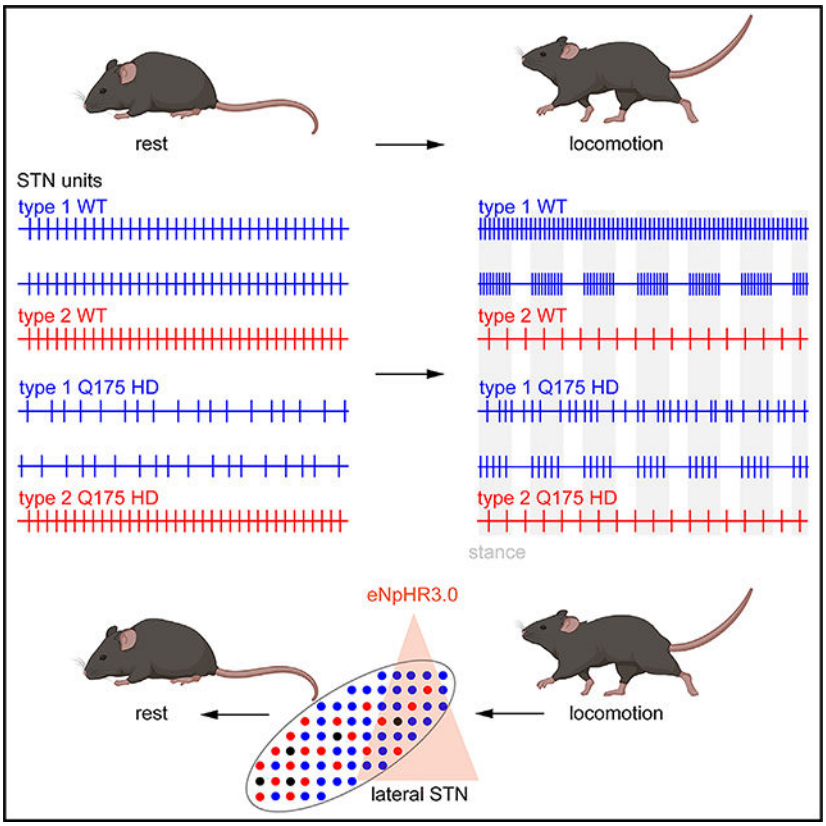

In brief

Callahan et al. find using electrophysiological recording and optogenetic inhibition that movement-related increases in the firing of type 1 subthalamic nucleus neurons are critical for normal locomotion and that gait impairments in Q175 Huntington's disease mice are specifically associated with the abnormal hypoactivity of type 1 cells.

INTRODUCTION

The glutamatergic subthalamic nucleus (STN) is a small but key component of the basal ganglia, a group of subcortical brain nuclei critical for habitual/automatic, goal-directed/flexible, and motivated behaviors.[1] The STN is classically thought to prevent, limit, or stop movement.[2–9] At rest, tonic driving of inhibitory basal ganglia output by the STN may suppress the activity of multiple motor centers.[2] In addition, hyperdirect and indirect pathway-mediated elevations in STN activity have been proposed to prevent an imminent action, terminate execution of an action, and/or facilitate execution of volitional movement through suppression of competing actions.[3–14] Consistent with these functions, (1) lesions or prolonged pharmacological, optogenetic, or chemogenetic inhibition of the STN leads to dyskinesia, hyperkinesia, premature or inappropriate responding, and stereotyped behaviors, such as excessive grooming[5,13,15–18]; (2) brief or prolonged optogenetic excitation of the STN typically prevents, reduces, or terminates movement,[7,9,11,17,19] but see Friedman et al.[20] and Fan et al.;[21] (3) a subset of STN neurons exhibit elevated activity during passive

or voluntary movement, whereas the activity of a partially overlapping subset of neurons is linked to stop, no go, or switch signaling.[6–14,22–27] Together, these data argue that the STN can suppress movement in some contexts but whether the STN actively facilitates the execution of volitional actions is less clear.[13,28–30]

The encoding properties of individual STN neurons are related to the cortico-basal ganglia thalamo-cortical loop(s) in which they reside.[8–11,13,23,24,26,27,31] Thus, movement-related activity is more prevalent in the dorsal and lateral STN, which is preferentially innervated by the motor cortex, and exhibits a somatotopic organization consistent with the anatomical arrangement of cortical afferents.[10,13,14,23,24,26,31–41] In contrast, no go, stop, and limbic signaling are more common in the ventral and medial aspects of the STN, which are more strongly innervated by prefrontal, limbic, and higher order motor cortical areas.[8,10,12,35,36,38,39,42] However, some STN neurons exhibit complex combinations of encoding properties presumably due to partial overlap of functionally heterogeneous cortico-STN terminal fields and STN neuron dendrites that traverse distinct functional zones, especially in rodents.[8,10,11,14,43] Consistent with this general framework, lesions or pharmacological/chemogenetic inhibition of the motor subthalamic region increase movement or produce dyskinesia/ballism, whereas more medially placed manipulations generate stereotyped behavior.[13,15–19,37] In addition to their functional diversity, STN neurons exhibit heterogeneous molecular properties; e.g., parvalbumin (PV)- and calretinin-expressing STN neurons are concentrated in the motor and limbic zones of the nucleus, respectively, arguing that these neuron subtypes subserve distinct functions.[44,45] Furthermore, adjacent PV-expressing and non-PV-expressing neurons in the dorsolateral STN have distinct connections and synaptic properties, arguing for additional STN functional subtypes and circuit complexity.[46]

Our understanding of STN function has been greatly informed by the impact of dysregulated STN activity in psychomotor disorders. In Parkinson's disease (PD), STN hyperactivity and/or excessive synchronization have been linked to akinesia, rigidity, and gait deficits.[2,27,47–49] In contrast STN hypoactivity has been proposed to underlie ballism and to contribute to chorea, gait abnormalities, and psychiatric symptoms in Huntington's disease (HD).[2,27,50–52] Deep brain stimulation (DBS) of the dorsolateral STN ameliorates akinesia, rigidity, and gait deficits in PD,[53,54] whereas DBS of the ventromedial STN reduces obsessive compulsive behavior[55] and can elicit affective and cognitive side effects in PD,[56,57] consistent with the STN's regional, anatomically based functional organization.

Much of the work described above studied rodents and non-human primates during the execution of highly trained licking behaviors and reaching, respectively, or human patients with neurologic/psychiatric disorders on and off therapy. The role of the STN in the execution of self-initiated, naturalistic behaviors like locomotion therefore remains an open question.[28] The effects of lesions or pharmacologic/optogenetic/chemogenetic manipulations to address a causative role for the STN in action execution or active stopping or the expression of disease symptoms have also been difficult to interpret due to their powerful, non-specific, prolonged, and irreversible or slowly reversible effects. Finally, given that the STN is a deep and highly vascularized structure, composed of small, tightly packed neurons, well-isolated recordings of individual neurons are technically

challenging,[25] especially under freely moving configurations. With these considerations in mind, we re-examined the role of the STN in motor control using silicon probe/optrode recordings in head-fixed mice at rest and during self-initiated, self-paced treadmill locomotion. Brief 5-s optogenetic inhibition was used to infer the impact of ongoing STN activity on rest or an already initiated locomotor bout. In addition, we compared STN encoding in wild-type (WT) mice with Q175 HD mice because Q175 mice exhibit subtle but consistent gait deficits that are analogous to those in patients with HD[58–61] and may in part reflect the dysregulated activity of STN neurons in HD and its experimental models.[50–52,62]

RESULTS

1–2 weeks after surgically affixing a metal plate to the skull, WT and Q175 mice were habituated to head fixation on a cylindrical or linear self-paced treadmill over 3–5 sessions (Figure 1A). After each habituation session, mice were returned to their home cage. Within one to two sessions, mice spontaneously locomoted in the forward direction interspersed with periods of rest or occasional sleep (Figure 1B). On the day of recording, mice were head-fixed. A 32- or 64-channel silicon probe/optrode was then advanced toward the STN, and electrophysiological recordings were made as mice rested and locomoted (Figure 1C). At the end of the recording session, mice were perfuse-fixed. Recording sites were assessed histologically (Figure 1D) and charted in 3 dimensions in the Allen Brain Atlas Common Coordinate Framework using NeuroInfo (MBF BioSciences).

Locomotor periods were defined as periods in which treadmill velocity was ≥0.25 cm/s for ≥200 ms (Figure 1B). Pre- and post-locomotor periods were defined as the second preceding and following a locomotor bout, respectively. Self-initiated locomotion was of higher velocity in WT and Q175 female mice (Table S1) compared to their male counterparts. As a result, phenotypic comparisons were made using datasets that were matched for sex (4 males and 3 females per group). Although both WT and Q175 mice locomoted spontaneously in the head-fixed configuration, locomotor performance was subtly but consistently impaired in Q175 mice, analogous to deficits in freely moving mice.[58–61] Thus, locomotor bouts were of lower velocity and shorter duration (Figures 1E–1H; Table S1). In some cases digital movies (100 fps) of the mice contralateral to the recorded hemisphere were taken during the recording session and movements of the forepaw and hindpaw were tracked using DeepLabCut[63,64] (Figures 1I–1N). Because tracking was most accurate and consistent for the contralateral hindpaw, locomotion kinematics were assessed from this body part. Although, the contralateral hindpaw exhibited similar trajectories during locomotion in WT and Q175 mice (Figures 1O and 1P; Table S1), stance- and swing-associated movements were of longer duration (Figures 1Q and 1R; Table S1) and associated with lower mean and peak velocities (Figures 1S–1V; Table S1) in Q175 mice. The interval between strides was also longer in Q175 mice (Figure 1W; Table S1).

To restrict our sample of STN activity to well-isolated single units, the following inclusion criteria were utilized: (1) PCA clusters were significantly different ($p < 0.05$); (2) J3-statistic was ≥1; (3) Davies Bouldin test statistic was ≤0.5. In addition, a threshold of <0.5% of interspike intervals under 2 ms was required for classification as a putative single unit (percent interspike interval within 2 ms; WT: 0.074, 0.0–0.2, $n = 99$; Q175: 0.0, 0.0–0.117,

n = 103; values represent median and interquartile range). 30-s periods of immobility prior to pre-locomotor periods were used to measure STN activity at rest. At rest, STN neurons in WT and Q175 mice discharged in a tonic but irregular firing pattern, as described previously[50] (Figure 2A; Table S2). However, the overall frequency of STN activity was lower in Q175 mice (Figures 2A–2C; Table S2), apparently due to a large increase in neurons discharging at frequencies below 5 Hz (Figure 2C; Table S2). The regularity of baseline activity, as assessed from the coefficient of variation (CV) of the interspike interval, was also significantly lower in Q175 than WT mice (Figures 2A and 2D–2F; Table S2), including those STN neurons that fired below 5 Hz or at 5 Hz and above (Figure 2F; Table S2).

The majority of STN neurons in WT and Q175 mice consistently exhibited locomotion-related changes in firing that were positively correlated with treadmill velocity (WT: 64.9%, 61 of 94 neurons; Q175: 69.3%, 52 of 75 neurons; Figures 3A–3N S1A, and S1B; Table S3). Units exhibiting these properties were defined as type 1 neurons. Overall, the firing frequency of type 1 units and their corresponding Z scores were greater in the pre-locomotion period versus rest, in the locomotion period versus the pre-locomotion and post-locomotion periods, and the post-locomotion period versus the subsequent rest period in both WT and Q175 mice (Figures 3F, 3G, 3M, 3N, and S1; Table S3). Spike frequency-treadmill velocity correlations ranged from weak to strong, and although they generally peaked close to 0 ms, they were temporally broad in nature (Figures 3C, 3D, 3J, and 3K). Close inspection of instantaneous spike frequency versus treadmill velocity within a locomotor bout revealed that even for strongly correlated neurons, spike frequency varied widely for identical treadmill velocities and conversely could be similar for quite different treadmill velocities (Figures 3E and 3L). Together, these data reveal that the majority of STN neurons exhibit locomotion-related increases in spiking activity that are positively correlated with treadmill velocity. However, the complexity of the instantaneous spike frequency-velocity relationship and the modest and temporally broad nature of the spike frequency-velocity correlation argue that additional aspects of locomotion are encoded by type 1 cells.

Consistent with previous observations in anesthetized mice,[50] the mean frequencies of type 1 STN activity in the rest, pre-locomotor, locomotor, and post-locomotor periods were lower in Q175 mice (Figure 4A; Table S4). This was accompanied by a reduction in spike frequency-treadmill velocity correlation (WT: 0.3456, 0.2205–0.5145; Q175: 0.2837, 0.1779–0.4094; p = 0.0348; Table S4) in Q175 mice relative to WT. In contrast, the respective Z scores for each period were not significantly different in WT and Q175 mice (Figure 4B; Table S4). Together, these data argue that locomotion-related, synaptic patterning of type 1 neurons is similar in WT and Q175 mice, but firing in response to synaptic input may be limited by the lower intrinsic excitability of STN neurons and hyperactivity of upstream prototypic GABAergic GPe neurons in Q175 mice, as described previously.[50,52] Although the frequency and CV of neuronal firing are often inversely related, spiking frequency and CV exhibited parallel locomotion-related changes in WT mice (Figure S1C). Thus, the synaptic mechanisms that underlie locomotion-related increases in activity additionally confer irregularity in WT mice. This trend was less apparent in Q175 mice (Figure S1D). Overall, these data reveal that during rest and the

pre-locomotor, locomotor, and post-locomotor periods, the frequency of type 1 unit activity is significantly lower in Q175 mice, although locomotion-related changes in activity are still present.

Recordings in WT were slightly biased to the lateral two-thirds of the STN (74.1%) compared to the medial third (25.9%), in contrast to recordings in Q175 mice, which sampled these sectors as one would predict from the relative sizes of these domains, i.e., 66.7% of electrode tracks were in the lateral two-thirds of the STN and 33.3% were in the medial third (Figures S1E and S1F). Adjusting the numbers of type 1 units for sampling bias in this dimension did not alter the conclusion that the majority of STN units are type 1 in WT mice (type 1 = 61.7%, 58 of 94 neurons). Furthermore, comparing the raw or adjusted numbers of type 1 units versus all other units revealed that type 1 units were concentrated in the lateral two-thirds of the STN in WT (WT raw: lateral STN type 1 = 54, not-type 1 = 17; medial STN type 1 = 7, not-type 1 = 16; $p < 0.001$, Fisher's test; WT adjusted: lateral STN type 1 = 49, not-type 1 = 16; medial STN type 1 = 9, not-type 1 = 20; $p < 0.001$, Fisher's test) but not Q175 mice (Q175 raw: lateral STN type 1 = 35, not-type 1 = 17; medial STN type 1 = 17, not-type 1 = 6; $p > 0.05$, Fisher's test) (Figures 4C and 4D). Whether in Q175 mice this represents a loss of type 1 encoding in lateral STN neurons, or a developmental shift in the spatial distribution of type 1 neurons or their afferents is unclear.

The activity of a subset of type 1 units was further analyzed with respect to contralateral limb kinematics during locomotion. 50% and 35% of units in WT and Q175 mice, respectively, exhibited firing that was related to the phase of the locomotor cycle, as assessed from histograms of spikes versus phase of locomotion (WT: $n = 6$ of 12 neurons; Q175: $n = 6$ of 17 neurons; Figures 4E–4I, S2A, and S2B; Table S4). Activity was highest during the stance or propulsive phase of the contralateral hindpaw locomotor cycle (Figures 4E–4I; Table S4). In neurons with phase-encoding, the total number of spikes per stance phase was lower in Q175 mice, reflecting the general hypoactivity of type 1 units in these mice (Figures 4E–4I; Table S4). 50% and 65% of units in WT and Q175 mice, respectively, exhibited firing that was not related to the phase of the locomotor cycle (WT: $n = 6$ of 12 neurons; Q175: $n = 11$ of 17 neurons; Figures S2A–S2G; Table S4). In these cases, spike counts were similar during the stance/propulsive and swing phases of the contralateral hindpaw locomotor cycle, as assessed from histograms of spikes versus phase of locomotion (Figures S2A–S2G; Table S4). In neurons without phase-encoding, the number of spikes per swing phase was lower in Q175 mice (Figures S2C–S2G; Table S4).

In WT and Q175 mice, a minority of STN neurons (type 2) consistently exhibited firing rates that decreased during locomotion whether adjusted for sampling bias in WT or not (WT raw: 27.7%, $n = 26$ of 94; Q175: 16.0%, $n = 12$ of 75; Figures 5, S3A, and S3B; Table S5) and were negatively correlated with treadmill velocity (Figures 5C, 5D, 5J, and 5K; Table S5). In contrast to type 1 neurons, the frequency of pre-locomotor activity was not significantly different from the preceding rest period (Figures 5F and 5M; Table S5). However, the frequency and associated Z scores, and precision of firing during locomotion were significantly lower than the pre-locomotor and post-locomotor periods (Figures 5F, 5G, 5M, 5N, S3C, and S3D). The firing rates and/or associated Z scores were also modestly but significantly elevated in the second following locomotion compared to the subsequent rest

period (Figures 5F, 5G, 5M, and 5N) in WT and Q175 mice. If the locomotion-associated dips in type 2 activity are due to synaptic inhibition, the elevated firing in the post-locomotor period could reflect post-inhibitory rebound firing, an intrinsic membrane property of most STN neurons.[65,66] In stark contrast to type 1 units, the frequency and pattern of type 2 neuron activity at rest and during locomotion were not significantly different in WT and Q175 mice (Figures 6A, 6B, S3C, and S3D; Table S6). Type 2 units were relatively prevalent in the medial STN of WT compared to the lateral STN, but exhibited no spatial preference in Q175 mice, whether corrected for sampling bias or not (WT raw: lateral STN type 2 = 14, not-type 2 = 57; medial STN type 2 = 12, not-type 2 = 11; $p = 0.030$, Fisher's test; WT adjusted: lateral STN type 2 = 13, not-type 2 = 52; medial STN type 2 = 15, not-type 2 = 14; $p = 0.0156$, Fisher's test; Q175 raw: lateral STN type 2 = 9, not-type 1 = 43; medial STN type 2 = 3, not-type 2 = 20; $p > 0.05$, Fisher's test) (Figures 6C and 6D). During locomotion the firing of type 2 neurons was not consistently related to the phase of the locomotor cycle and the numbers of spikes per stance and swing phase were similar in WT and Q175 mice (Figures 5E, 5L, and 6E–6I; Tables S5 and S6). Together these data demonstrate that in contrast to type 1 neurons, the rate and pattern of type 2 neuron activity both at rest and during locomotion are similar in WT and Q175 mice. The firing of a small proportion of STN neurons was uncorrelated with locomotion (WT: 7.4%, $n = 7$ of 94 neurons; Q175: 14.7%, $n = 11$ of 75 neurons). The spatial distribution of these neurons did not exhibit a preference for the lateral or medial STN in WT or Q175 mice (Figure 6C).

Several studies have revealed that the molecular properties of STN neurons are heterogeneous, e.g., subtypes of STN neurons differentially express the calcium binding protein parvalbumin (PV) or the type 2 vesicular glutamate transporter (vGluT2) and exhibit distinct membrane and synaptic properties.[44–46] To determine whether molecularly defined STN subtypes are correlated with STN subtypes defined by their locomotion-encoding properties, STN subtypes were optogenetically tagged. The encoding properties and non-specific effects of light delivery were first established in control WT mice in which eGFP was virally expressed in STN neurons through injection of AAVs carrying a synapsin promoter-dependent construct (Figures S4A, S4B, S4F, S4G, S4H, S4K, S5A, and S5B; Table S7). In the absence of opsin expression, 633 nm light delivery had no consistent effect on the activity of 11 units that were recorded (Figures S4F, S4G, and S5A; Table S7). Of these 11 units, 8 exhibited type 1 activity, 2 exhibited type 2 activity, and 1 was uncorrelated with locomotion (Figures S4H, S4K, and S5B; and Table S7), similar to the proportions of encoding subtypes described above.

To determine whether PV expression is correlated with the locomotion-encoding subtypes described above, eNpHR3.0-eYFP or ChR2(H134R)-eYFP was expressed in PV+ STN neurons through injection of AAV vectors carrying Cre-dependent constructs into the STN of PV-Cre mice (Figures S4A, S4C, S4D, S4F, S4G, S4I, S4L, S5C, S5D, S5E, and S5F; Table S7). Silicon optrodes were then used to optotag/identify and record the activity of STN PV+ neurons at rest and during locomotion (Figures S4A, S4C, S4D, S4F, S4G, S4I, S4L, and S5C–S5F; Table S7). Using this approach 11 neurons were optotagged. Of these 9 exhibited type 1 neuronal activity and 2 exhibited type 2 neuronal activity (Figures S4I, S4L, and S5F; Table S7). A similar approach was used to determine whether the subset of STN neurons that express vGluT2 exhibit distinct encoding properties.[46] In

this case the inhibitory opsin eNpHR3.0-eYFP was virally expressed in a Cre-dependent manner in vGluT2-Cre mice (Figures S4A, S4E, S4F, S4G, S4J, S4M, S5G, and S5H; Table S7). Using this approach, 11 neurons were optotagged. Of these 7 exhibited type 1 neuronal activity and 3 exhibited type 2 neuronal activity and 1 exhibited activity that was uncorrelated with locomotion (Figures S4J, S4M, and S5H; Table S7). Given that the proportions and distributions of optotagged STN neurons exhibiting type 1 or type 2 neuronal activity were similar to neurons expressing eGFP (Figures S5I and S5J; Table S7) or non-expressing neurons described above, we conclude that neither PV or vGluT2 expression reliably distinguishes between STN neurons with type 1 or 2 locomotor encoding properties. The baseline and locomotion-associated activities and locomotion-associated Z scores of identified PV+ and vGluT2+ STN neurons were also not significantly different from each other or eGFP-expressing STN neurons (Figures S5K, S5L, and S5M; Table S7).

To determine the functional role of locomotion-associated STN activity, the inhibitory opsin eNpHR3.0-eYFP was virally expressed in vGluT2-Cre mice through subthalamic injection of AAVs carrying a Cre-dependent construct, as described above (Figures S4A and S4E), or in WT mice through subthalamic injection of AAVs carrying a CaMKII-dependent expression construct (Figures S6A–S6D). To control for the effects of viral expression and light delivery, eGFP alone was expressed in the STN in a subset of WT mice, as described above (Figures S4A and S4B). 32–64 channel silicon optrodes were then used to record and unilaterally inhibit STN activity for 5-s in mice at rest or during a self-initiated locomotor bout (Figures 7 and S6; Table S8). Data from WT or vGluT2-Cre mice were pooled because activation of eNpHR3.0-eYFP inhibited STN activity similarly (Figure S6E; Table S8). Application of 633 nm light in eGFP-expressing WT mice had no effect on STN unit activity, as described above (Figures S4F and S4G; Tables S7 and S8). Consistent with the majority of neurons in the lateral two-thirds of the STN being type 1 (Tables S4 and S6), optogenetically inhibited neurons in this sector were predominantly type 1 encoding (type 1, 90.9%; type 2 9.1%; uncorrelated, 0%; Figure S6F; Table S8). In contrast, in the medial third of the STN where encoding subtypes are more evenly represented (Figure S6F; Tables S4 and S6), optogenetically inhibited STN neurons were a mixture of subtypes (type 1, 27.3%; type 2, 45.4%; uncorrelated, 27.3%; Table S8). Optogenetic inhibition of the lateral two-thirds or medial third of the STN or distinct encoding subtypes suppressed unit activity to a similar degree (Figures 7A and 7B; Table S8).

Optogenetic inhibition of the lateral or medial STN or equivalent light delivery in eGFP-expressing control mice had no effect at rest arguing that reduction of type 2 STN activity is not sufficient for locomotion initiation, (Figures 7C and 7D; Table S8). Optogenetic inhibition of the medial third of the STN also had no significant effect on coincident locomotion relative to the effects of identical light delivery in eGFP-expressing control mice (Figures 7E and 7F; Table S8). However, optogenetic inhibition of the lateral two-thirds of the STN interrupted coincident locomotion compared to the effects of similarly directed, timed, and intensities of light in eGFP-expressing mice (Figures 7E–7N; Table S8). Optogenetic truncation of locomotion was associated with either abrupt time-locked cessation of locomotion, progressive slowing of locomotion before bout termination, and in some cases dysregulated limb movement, including reverse locomotion (Figures 7G–7K; Table S8). Given the small size of the STN and the potential for light to spread in the

mediolateral axis, the regional effects of optogenetic inhibition were further analyzed. Optogenetic inhibition with fiberoptics placed over the lateral or central third of the STN truncated locomotor bouts to a similar degree versus optogenetic inhibition with fiberoptics over the medial third of the STN or light delivery alone (Figure S6G; Table S8). Together these data confirm that only optogenetic inhibition of the lateral two-thirds of the STN disrupts locomotion. Optogenetic inhibition similarly truncated locomotion in WT and vGluT2-Cre mice (Figure S6H; Table S8) and did not have cumulative effects on locomotion (Figure S6I; Table S8) because locomotor bouts that coincided with optogenetic inhibition in the first 50% or subsequent 50% of trials were of similar duration. Optogenetic inhibition of the lateral two-thirds of the STN also significantly disrupted contralateral hindpaw kinematics (Figures 7L–7N; Table S8). Thus, the duration of the stance phase of the locomotor cycle (Figure 7L; Table S8) increased, the velocity of the stance phase decreased (Figure 7M; Table S8), and the interval between strides increased (Figure 7N; Table S8). Together, these data argue that 1) locomotion-locked type 1 unit activity in the lateral STN contributes to optimal locomotor performance 2) optogenetic inhibition of the lateral STN induces locomotor effects analogous to the deficits seen in Q175 mice, in which the activity of type 1 STN neurons both at rest and during locomotion are reduced relative to WT.

DISCUSSION

Similar to studies of arm movement-related subthalamic activity in primates,[8,10,13,24,26] in mice the majority of STN neurons (type 1) exhibited locomotion-dependent increases in activity. Although type 1 units (by definition) exhibited significant spike rate/treadmill velocity correlations, associated Pearson's coefficients ranged from weak (0.1) to strong (0.7), presumably because the relationships between spike rate and treadmill velocity *within* a stride cycle or locomotor bout were inconsistent with units exhibiting very different spike rates for identical velocities. Furthermore, although spike rate/velocity correlations peaked close to 0 ms, velocity encoding was temporally imprecise because correlation strength decayed modestly over a second. Together, these data argue that type 1 STN neurons encode additional aspects of volitional movement. Consistent with this possibility 1) 50% of type 1 neurons exhibited activity that was highest during the propulsive phase of the contralateral locomotor cycle 2) arm movement-related changes in STN discharge exhibit direction selectivity and/or correlate with movement amplitude/velocity in monkeys[14,24,26,27] 3) changes in STN beta band activity are correlated with the onset, execution, vigor, phase, and termination of bipedal locomotion in human PD patients.[28,30] Finally, type I neurons may also encode movements that are less directly linked to locomotion such as axial postural adjustments, and/or micromovements unrelated to locomotion itself.[67]

Type 1 units typically exhibited increases in activity several hundred milliseconds prior to the onset of locomotion, consistent with several studies that detected elevations in STN activity prior to arm movement and associated changes in EMG.[14,26] These data suggest that type 1 activity is driven at least in part by motor command signals emanating from motor cortical regions. Following the end of each locomotor bout, type 1 activity decreased in a time-locked fashion. However, activity remained modestly elevated during the second following locomotion. This persistent elevation of firing may reflect ongoing activity in

upstream nuclei related to post-locomotion postural adjustments and/or the slow decay of metabotropic receptor-mediated afferent synaptic transmission.

In concordance with previous studies and the distribution of cortical inputs, type 1 units were concentrated in the lateral two-thirds of the STN in WT mice. The circuits driving locomotion-related type 1 activity are potentially complex because the STN receives inputs from motor command structures such as the primary motor cortex and mesencephalic locomotor region and sensory/proprioceptive information via the cortex, parafascicular thalamic nucleus, and brainstem.[30,68–71] Indeed, neurons in the lateral STN respond to both motor cortical stimulation with short latency excitation, consistent with monosynaptic driving,[13,23,38] and to passive limb movement with increased activity, consistent with proprioceptive encoding.[8,24,26,30] It is also likely that indirect pathway-mediated striatopallidal inhibition of prototypic globus pallidus (GPe) neurons leads to disinhibition of STN type 1 neurons during locomotion.[23,38,72,73] Indeed, neurons in the lateral STN also respond to motor cortical stimulation with a second longer latency and duration excitation due to indirect pathway-mediated disinhibition.[23,38,39] A recent study suggests that parafascicular thalamic inputs to the STN can also potently drive locomotion under some conditions.[71]

Approximately 28% of STN neurons consistently exhibited locomotion-locked reductions in activity across locomotor bouts in WT mice. In contrast to type 1 units, changes in type 2 activity were restricted to the locomotor period only. Type 2 units exhibited negative weak to strong spike rate/treadmill velocity correlations that were temporally broad. As for type 1 neurons, the relationships between spike rate and treadmill velocity within a locomotor bout were inconsistent. However, the locomotor cycle was not well represented by type 2 activity, presumably due to its sparsity. Together, these data argue that reductions/cessations in type 2 activity encode the period rather than the parameters of locomotion. Type 2 units were distributed across the mediolateral axis of the STN and were often recorded concurrently with type 1 units. STN units with movement-related reductions in firing have also been reported for upper limb movement in primates and were similarly rare.[13,24,26] One possibility is that type 2 neurons encode the movement of body parts unrelated to locomotion, and their activity is suppressed by a combination of low motor command/proprioceptive drive and/or increased inhibition from disinhibited prototypic GPe neurons that are not targets of striatopallidal inhibition.[72,74,75] Another possibility is that some of these neurons, particularly in the medial third of the nucleus, signal the stopping or switching of actions and are suppressed by low drive from stop/switch-encoding cortical areas (e.g., dorsomedial prefrontal cortex) and/or increased inhibition from disinhibited prototypic GPe neurons that are not subject to striatopallidal inhibition.[9,36] The relatively large proportion of STN neurons exhibiting locomotion-related activity in WT mice compared to contralateral arm-related activity in primates[8,10,24,26,34] may reflect the involvement of all four limbs in quadrupedal locomotion and a lower degree of somatotopic specificity in rodents.[23,31,35] Less than 10% of STN units were uncorrelated with locomotion. Given their lack of engagement in movement encoding, these neurons may exclusively convey stop or switch signals from cortical areas such as the dorsomedial prefrontal cortex.[8,10,12,23,38,39]

Multiple studies have demonstrated that STN neurons are heterogeneous in their molecular properties.[44–46] In many brain nuclei, this molecular diversity delineates cell classes that are embedded in distinct circuits that subserve specific functions.[76] To address this possibility, we optotagged PV- or vGluT2-expressing neurons and measured their activity at rest and during locomotion. Although these neuron classes exhibit distinct membrane and synaptic properties and spatial distributions and subserve distinct functions in some contexts,[46] PV- and vGluT2-expressing neurons were composed of both type 1 and 2 STN neurons. Thus, PV and vGluT2 expression in the STN are unreliable markers of movement encoding and presumably confer molecular specializations related to other aspects of circuit function, e.g., motor learning.[46]

Q175 and other HD mouse models exhibit progressive movement and gait deficits that mimic those seen in human patients, e.g., reductions in locomotion velocity, stance and swing velocity, and stride coordination, and increases in inter-stride interval.[59–61] Consistent with these deficits, head-fixed Q175 mice exhibited relatively short durations and low velocities of locomotion, low-velocity paw kinematics, and increased time between strides. These deficits were specifically associated with abnormal hypoactivity of type 1 STN neurons both at rest and during locomotion. Previous studies utilizing *ex vivo* brain slices from Q175 mice or anesthetized Q175 mice revealed that a subset of STN neurons exhibit hypoactivity relative to WT mice.[50,52] This hypoactivity was caused by (1) NMDA receptor-dependent mitochondrial oxidant stress and increased activation of K_{ATP} channels by reactive oxygen species (ROS)[52] (2) hyperactivity of upstream GABAergic GPe neurons.[50] Given that locomotion-associated increases in STN activity could arise from increased glutamatergic drive from motor command and proprioceptive structures and disinhibitory signaling from the GPe, the hypoactivity of type 1 neurons in Q175 mice may reflect increased NMDA receptor and ROS-dependent activation of K_{ATP} channels *and* pathological hyperactivity of upstream GPe neurons. Consistent with these mechanisms, (1) mitochondrial oxidant stress, ROS generation, and K_{ATP} channel activation are elevated in *ex vivo* brain slices from Q175 mice[52]; (2) although optogenetic inhibition of prototypic GPe neurons disinhibited STN activity in both anesthetized WT and Q175 mice, STN activity remained lower in Q175 mice.[50]

To determine the role of the STN in regulating locomotor activity, we optogenetically inhibited the STN of WT mice for 5 s at rest or during locomotion. No effect of optogenetic inhibition was observed in resting mice, arguing that STN hypoactivity generally and cessation of type 2 neuron activity specifically are not sufficient to initiate locomotion. At first sight, this observation appears contrary to the effects of STN lesions or prolonged pharmacological/optogenetic/chemogenetic inhibition of the STN.[5,13,15–18] However, the dysregulated movement that accompanies STN lesions or prolonged subthalamic inhibition may require volitional motor commands for its expression. If correct, the short duration of the optogenetic inhibition utilized here may have sufficiently reduced the probability of coincident action initiation/execution that the behavioral impact of STN inhibition was not revealed. Consistent with this hypothesis, brief optogenetic inhibition of the STN rapidly dysregulated self-initiated locomotor bouts that were already in the process of execution. Importantly this effect was restricted to the inhibition of the lateral STN where type 1 units are concentrated. Analogous dysregulation of a highly trained action

sequence or spontaneous behavior accompanies bidirectional optogenetic manipulation of upstream components of the indirect pathway/network[77] and is in line with reports that concomitant, coordinated direct *and* indirect pathway activity is necessary for optimal volitional movement.[78–80] Thus, rather than simply stopping movement,[81] indirect pathway nuclei, including the STN, play key roles in movement execution.

Precisely how type 1 STN activity optimizes self-initiated locomotion remains to be tested. One possibility is that widespread inhibition of movement generation/regulation circuits by the indirect and hyperdirect pathways that flow through the STN enhances the functional impact of selective direct pathway-mediated disinhibition of locomotion-generating circuitry.[4,13,82] That said, the richness of locomotor cycle encoding by 50% of type 1 neurons argues that the indirect and hyperdirect pathways may also play a more dynamic and active role in kinematic regulation than previously supposed,[83] e.g., by terminating direct pathway-mediated inhibition of basal ganglia output neurons.[13] Another possibility is that type 1 STN activity promotes locomotion through excitation of dorsal striatum-projecting substantia nigra (SN) dopamine neurons, which in turn mediate D1 dopamine receptor-dependent enhancement of direct pathway striatal projection neuron excitability and synaptic integration,[21,84–86] but see Markowitz et al., da Silva et al., and Coddington and Dudman.[87–89] However, optogenetic inhibition of SN dopamine neurons does not dysregulate motor sequences already in the process of execution,[88] arguing that the rapid impact of STN inhibition on locomotion is unrelated to interruption of the STN's excitation of dopamine neurons.

How do the findings described here inform our understanding and treatment of movement disorders? Together with other studies, our data support the conclusion that type 1 STN activity helps to optimize gait and that dysregulation of this activity in HD or PD contributes to gait deficits in these movement disorders. In HD, the cell-autonomous effects of mutant huntingtin directly compromise the encoding and survival of a subset of STN neurons,[50,52,62] arguing that treatments that suppress mutant huntingtin expression[90] should be targeted widely and not focused solely on the striatum or cortex for full circuit/functional rescue. In PD, incomplete restoration of subthalamic locomotor encoding may contribute to the mixed effects of repetitive high-frequency DBS of the STN on gait deficits.[91] Indeed, coordinated reset stimulation[92] or locomotor cycle-dependent stimulation[28] that restore or impose more natural patterns of STN activity, respectively, may have the potential to rescue gait more consistently than traditional STN DBS.

Limitations of the study

The major limitation of this work is the absence of genetic tools that could be used to distinguish the functional roles of type 1 and 2 STN neurons. To circumvent this, optogenetic inhibition was directed to sectors of the STN where type 1 units were the major cell type (lateral STN) or type 2 neurons comprised the majority (medial STN). Although optogenetic inhibition of type 2 neurons was partly occluded by locomotion-associated suppression, optogenetic inhibition suppressed type 2 activity completely. Thus, optogenetic inhibition of type 2 activity in the lateral STN may have contributed to locomotor dysregulation. Similarly, optogenetic suppression of type 1 activity in WT mice was more

severe than the hypoactivity of these neurons in Q175 mice. Another limitation of our work is that the circuit elements responsible for the generation of movement-related STN activity remain to be determined.

STAR★METHODS

Detailed methods are provided in the online version of this paper and include the following:

RESOURCE AVAILABILITY

Lead contact—Further information and requests for resources and reagents should be directed to and will be fulfilled by the lead contact, Mark Bevan (m-bevan@northwestern.edu).

Materials availability—This study did not generate new unique reagents. All materials are available from the commercial vendors listed in the key resources table.

Data and code availability—All data reported in this paper will be shared by the lead contact upon request. This paper does not report original code. Any additional information required to reanalyze the data reported in this paper is available from the lead contact upon request.

EXPERIMENTAL MODEL AND STUDY PARTICIPANT DETAILS

Animals—Adult male and female heterozygous Q175 mice (B6.129S1-Htt$^{tm1.1Mfc}$/190ChdiJ; RRID:IMSR_JAX:029928; The Jackson Laboratory, Bar Harbor, ME, USA) and their wild-type (WT; C57B6/J; RRID:IMSR_JAX:000664; The Jackson Laboratory) littermates were used in this study (Q175: 251.0, 225.0–264.5 days old, n = 5 male, 4 female; WT: 223.0, 211.3–232.8 days old, n = 6 male, 6 female). For optogenetic experiments, adult male and female heterozygous Vglut2-ires-Cre knock-in mice (B6J.129S6(FVB)-Slc17a6$^{tm2(cre)Low}$/MwarJ; RRID:IMSR_JAX:028863; The Jackson Laboratory; 139, 134.0–187.5 days old; n = 1 male, 3 female) and PV-Cre mice (B6.Cg-Pvalb$^{tm1.1(cre)Aibs}$/J; RRID:IMSR_JAX:012358; The Jackson Laboratory; 145.5, 135.8–147.8 days old; n = 2 male, 2 female) were used. Data from male and female mice were overlapping and therefore pooled. Mice of the same sex were housed 1–5 per cage, maintained on a 14 h light/10 h dark cycle (conventional light cycle) or a 12 h dark/12 h light cycle (reverse light cycle) with food (standard mouse chow) and water available *ad libitum*. Housing temperature and humidity were maintained at 70–74°F and 30–70%, respectively. Measurements from mice in the dark (active) and light (inactive) phases of their light cycle were overlapping and therefore pooled, except for kinematic measurements, which were only made in mice during the dark (active) phases of their light cycle. Mice were monitored regularly by animal care technicians, veterinarians, and research staff. All procedures were performed in compliance with the policies of the National Institutes of Health and approved by the Institutional Animal Care and Use Committee of Northwestern University.

METHOD DETAILS

Stereotaxic injection of viral vectors—Before and after surgical procedures, lab surfaces and equipment were disinfected with 5% Nolvasan Surgical Scrub (Zoetis, Inc., Kalamazoo, MI, USA). All surgical instruments were autoclaved, and sterility was maintained throughout surgery. Anesthesia was induced with vaporized 3–4% isoflurane (Smiths Medical ASD, Inc., Dublin, OH, USA) followed by an intraperitoneal injection of ketamine (100 mg/kg in 0.9% saline solution). The fur overlying the dorsal surface of the head was shaved using hair clippers (Wahl, Sterling, IL, USA). Ophthalmic ointment (Covetrus, Portland, ME, USA) was applied to prevent corneal drying. The mouse was transferred to a stereotaxic apparatus (Neurostar, Tübingen, Germany) and placed on a thermal heating pad (Physitemp, Clifton, NJ, USA) covered in a sterile drape. The animal's head was secured in the stereotaxic frame with ear bars and anesthesia was maintained with 1–2% isoflurane. Depth of anesthesia was assessed by toe pinch throughout the procedure. The scalp was disinfected with 70% ethanol (Medline, Northfield, IL, USA) and Betadine (Dynarex Corporation, Orangeburg, NY, USA) and the skull was exposed with a single scalpel cut along the midline. AAVs diluted in sterile-filtered HEPES-buffered synthetic interstitial fluid (HBS SIF: 140 mM NaCl, 23 mM glucose, 15 mM HEPES, 3 mM KCl, 1.5 mM $MgCl_2$, 1.6 mM $CaCl_2$; pH 7.2 with NaOH; 300–310 mOsm/L) were then injected under stereotaxic guidance. eNpHR3.0-eYFP was virally expressed in the STN of WT mice through unilateral injection of AAV9-CaMKIIa-eNpHR3.0-eYFP (RRID:Addgene_26971; diluted to 2.4–4.8 × 10^{12} genome copies (GC)/mL; coordinates relative to bregma, AP: −1.90 mm; ML: 1.60 mm; DV: 4.60 mm; 0.3 μL). eNpHR3.0-eYFP was also virally expressed in the STN of vGluT2-Cre mice through unilateral injection of Cre-dependent AAV9-Ef1a-DIO-eNpHR3.0-eYFP (RRID:Addgene_26966; diluted to 1.9–4.4 × 10^{12} genome copies (GC)/mL; coordinates relative to bregma, AP: −1.90 mm; ML: 1.60 mm; DV: 4.60 mm; 0.3 μL). eNpHR3.0-eYFP or ChR2(H134R)-eYFP was virally expressed in PV-expressing STN neurons in PV-Cre mice through unilateral injection of Cre-dependent AAV9-Ef1a-DIO eNpHR3.0-eYFP (RRID:Addgene_26966; diluted to 1.9–4.4 × 10^{12} genome copies (GC)/mL; coordinates relative to bregma, AP: −1.90 mm; ML: 1.60 mm; DV: 4.60 mm; 0.3 μL) or AAV9.EF1a.DIO.hChR2(H134R)-eYFP.WPRE.hGH (RRID:Addgene_20298; diluted to 2.4 × 10^{12} genome copies (GC)/mL; coordinates relative to bregma, AP: −1.90 mm; ML: 1.60 mm; DV: 4.60 mm; 0.3 μL), respectively. Finally, eGFP was virally expressed in STN neurons through unilateral injection of AAV9-hSyn-eGFP (RRID:Addgene_50465; diluted to 2.0 × 10^{12} genome copies (GC)/mL; coordinates relative to bregma, AP: −1.90 mm; ML: 1.60 mm; DV: 4.60 mm; 0.3 μL). AAV injections were conducted over 10 min. The injectate was then allowed to diffuse for 10 min before the syringe was slowly retracted. The scalp was then sutured using nylon surgical sutures (6–0) (Henry Schein, Melville, NY, USA) and an analgesic, meloxicam (20 mg/kg in 0.9% saline solution) was administered by subcutaneous injection. After surgery mice were removed from the stereotaxic instrument and returned to their home cage. Cages were placed on an electric heating pad (Sunbeam Products, Boca Raton, FL, USA) until animals were ambulatory. The period between AAV injection and neuronal recording was between 2 and 4 weeks. Surgical methods are also available at: https://doi:10.17504/protocols.io.q26g7yr78gwz/v1.

Headplate implantation—Each mouse was prepared and anesthesia was induced, maintained, and assessed as for AAV injection. The skin overlying the cranium was removed using fine surgical scissors (Fine Science Tools, Foster City, CA, USA) such that the cranial suture points between bregma and lambda were exposed. Cotton tipped applicators were used to peel away the periosteum from the exposed cranium. To enhance the bonding of dental cement (Parkell, Inc., Edgewood, NY, USA) to the cranium, the surface of the skull was then gently scored with a handheld micromotor drill (Stoelting Co, Wood Dale, IL, USA). The micromotor drill was then used to drill a burr hole in the cranium above the STN (coordinates relative to bregma, AP: −1.90 mm; ML: 1.60 mm). A thin layer of Kwik-Sil silicone sealant (World Precision Instruments, Sarasota, FL, USA) was applied to bregma and the craniotomy overlying the STN to prevent the stereotaxic reference point and craniotomy from being exposed to dental cement. Kwik-Sil was allowed 1–2 min to cure before proceeding. A separate craniotomy was made above the cerebellum (coordinates relative to bregma, AP: −6.75 mm; ML: 0.80 mm). The dura was then carefully removed using a bent injection needle and a peridural screw electrode (MS51960–1; McMaster-Carr, Elmhurst, IL, USA) was affixed in place. A custom-designed titanium headplate (25.4 mm length × 9.4 mm width × 0.8 mm thickness) with a 5.8 mm × 3.0 mm oval opening was used for head-fixation. The headplate was attached to a custom holder mounted to the stereotaxic frame. A thin layer of dental cement was then applied to the skull and base of the peridural screw electrode to cover the exposed skull and provide a foundation for affixing the headplate. Another layer of dental cement was then applied to affix the headplate, leaving only the Kwik-Sil enclosed craniotomy above the STN and screw electrode exposed. Dental cement was allowed to dry and harden for 10 min. Following headplate implantation, an analgesic was administered and mice were allowed to recover as for AAV injection. Headplate implantation procedures are also available at: https://doi.org/10.17504/protocols.io.bp2l694z5lqe/v1.

Treadmill habituation and behavior—Seventy-two hours or more after head plate implantation and one week prior to *in vivo* electrophysiological recording, mice were habituated to head-fixation on a cylindrical or linear treadmill. The cylindrical treadmill comprised a Styrofoam cylinder (16.5 cm in diameter × 15 cm wide) with a stainless-steel axle (1257K46; McMaster-Carr). Ball bearings (4262T11; McMaster-Carr) affixed to the ends of the axle were used to reduce friction. An axle-mounted optical encoder (E2; US Digital, Vancouver, WA, USA) was used to sample treadmill velocity at 1000 Hz. The axle of the cylindrical treadmill was supported via custom mounts affixed to a vibration isolation table (Ametek TMC, Peabody, MA, USA). The linear treadmill (SpeedBelt; Phenosys, Berlin, Germany) consisted of a fabric belt (60 cm length × 7.5 cm width) wrapped around two wheels on which ball bearings were mounted to reduce friction. An optical motion sensor was used to sample treadmill velocity at 1000 Hz.

Experiments were initially conducted during the light period of the light-dark cycle but were subsequently transitioned to the dark period when mice are more active. Mice were briefly placed in an anesthetic induction chamber (2–3% isoflurane) and then quickly transferred to the cylindrical or linear treadmill. Headplates were secured to custom-made clamps on each side of the head. Head-fixation posts and clamps were fabricated from commercially

available components (Thorlabs, Newton, NJ, USA, and Luigs & Neumann, Ratingen, Germany). The final position of the headplate was typically 2.5–3.0 cm above the treadmill.

Digital movies were collected using 2 high-definition cameras (BFS-U3-04S2M-CS; Teledyne FLIR, Wilsonville, OR, USA) mounted to the front and side (contralateral to electrophysiological recording sites) of head-fixed mice. Frames were captured at 100 fps (720 × 540 pixels) using SpinView software (Spinnaker SDK; Teledyne FLIR). An infrared light source (CMVision, Houston, TX, USA) was used for illumination.

For experiments conducted using the cylindrical treadmill, habituation consisted of 3 sessions on consecutive days. The first session lasted for 30 min and subsequent sessions lasted for 60 min. On the first day of habituation mice attempted frequent postural adjustments and ambulated in both the forward and reverse directions. For experiments conducted using the linear treadmill, habituation consisted of five sessions on consecutive days. The first session lasted for 30 min and subsequent sessions lasted for 60 min. Over the course of habituation mice more consistently exhibited stereotyped and longer duration forward locomotion. After the conclusion of each habituation session, the animal's headplate was detached from the headplate clamps and the mouse was returned to its home cage. Procedures for treadmill habituation and measuring treadmill behavior are also available at: https://doi.org/10.17504/protocols.io.14egn2xrqg5d/v1.

***In vivo* electrophysiology and optogenetics—**The week following treadmill habituation, *in vivo* electrophysiological experiments were performed. Mice were head-fixed as described above. Using fine point forceps (Dumont #7 Forceps, Curved, Dumostar, 0.17 × 0.1 mm, 11.5 cm; Fine Science Tools) Kwik-Sil was carefully detached from the skull to expose both bregma and the craniotomy overlying the STN. Dura was carefully removed from the STN craniotomy using a bent syringe needle (25G). The craniotomy was then irrigated with HBS to prevent dehydration of exposed cortical tissue. Extracellular single-unit recordings were acquired using silicon probes and optrodes (A1×32-Poly3-10mm-50-177-A32 and A1×32-Poly3-10mm-50-177-OA32LP; NeuroNexus Technologies, Ann Arbor, MI; ASSY-77 Acute 64 channel H5 probe; Cambridge NeuroTech, Cambridge, UK) connected to a 64-channel Digital Lynx data acquisition system via a unity gain headstage (Neuralynx, Bozeman, MT, USA). Probes/optrodes were attached to a single-axis motorized micromanipulator (Scientifica, Uckfield, United Kingdom) that was mounted onto a 3-axis stereotaxic manual manipulator (David Kopf Instruments, Tujunga, CA, USA). The motorized micromanipulator was used to move probes/optrodes in the vertical axis and controlled using a PatchPad and LinLab software (Scientifica). The reference channel of the headstage was connected to the peridural screw electrode overlying the cerebellum by an insulated wire and signals were sampled at 40 kHz, with a gain of 14x. Online digital finite impulse response filters were applied. Single-unit activity was bandpass-filtered between 200 and 9000 Hz, and local field potential signals were bandpass-filtered between 0.1 and 400 Hz. A 633 nm direct diode laser (LuxX+ 633–100; Omicron-Laserage Laserprodukte, Rodgau, Germany) or a 473 nm direct diode laser (LuxX+ 473–100; Omicron-Laserage Laserprodukte) were used as light sources for optogenetic stimulation. An Axon Digidata 1440A (Molecular Devices, San Jose, CA, USA) and Clampex 11 software (Molecular Devices) were used to record treadmill velocity and

synchronize video capture, optogenetic light delivery, and electrophysiological recording. eNpHR3.0-eYFP-expressing STN neurons were optogenetically inhibited through delivery of 633 nm light (<6 mW) for a duration of 5 s. Stimulation was repeated 4 times with each trial of stimulation separated by 2 min. ChR2(H134R)-eYFP-expressing STN neurons were optogenetically stimulated using 10 ms pulses of 473 nm light (<6 mW) delivered at 0.2 Hz for 250 s. Laser intensity was calibrated as power at the tip of the optrode before implantation and verified at the conclusion of each experiment. In order to histologically verify recording sites, probe/optrode tracks were visualized postmortem by lightly dipping silicon probes in a lipophilic florescent dye (DiI; 20 mg/mL in 50% acetone/methanol; D282; Thermo Fisher Scientific, Waltham, MA, USA) prior to implantation or by immunohistochemical detection of the microglial marker, Iba1 (FUJIFILM Wako Pure Chemical Corporation, Richmond, VA, USA; RRID:AB_839504). Procedures for *in vivo* electrophysiology and optogenetic manipulation are also available at: https://doi.org/10.17504/protocols.io.rm7vzbn94vx1/v1.

Immunohistochemistry and confocal imaging—Following electrophysiological recording mice were given a lethal dose of anesthetic and then perfused transcardially with ~5–10 mL of 0.01 M phosphate buffered saline (PBS) (pH 7.4; P3813; MilliporeSigma, Burlington, MA, USA) followed by 15–30 mL of 4% paraformaldehyde (PFA) in 0.1 M phosphate buffer (PB), pH 7.4. Each brain was then removed and postfixed overnight in 4% PFA (in 0.1 M PB, pH 7.4) before being washed in PBS, blocked, and sectioned in the coronal or sagittal plane at 70 μm with a vibratome (VT1000S; Leica Biosystems Inc., Buffalo Grove, IL, USA). Sections were then processed for the immunohistochemical detection of NeuN, an antigen expressed by neurons that is commonly used to delineate brain structures. First, sections were washed in PBS and incubated for 48–72 h at 4°C in anti-NeuN (1:500; Abcam, Cambridge, United Kingdom; RRID:AB_10711040) and, if applicable, anti-Iba1 (1:1000) in PBS with 0.3% Triton X-100 (MilliporeSigma) and 2% normal donkey serum (Jackson ImmunoResearch Laboratories, Inc., West Grove, PA, USA). Then, sections were washed in PBS before being incubated for 90 min at room temperature in Alexa Fluor 405, 488-, 594-, or 647-conjugated donkey anti-mouse or anti-rabbit IgG (1:250; Thermo Fisher Scientific; RRID:AB_2884884; Jackson ImmunoResearch Laboratories; RRID:AB_2313584; RRID:AB_2340621; RRID: AB_2492288, RRID: AB_2340846, RRID: AB_2340854, RRID: AB_2340863) in PBS with 0.3% Triton X-100 and 2% normal donkey serum. Finally, sections were washed in PBS and mounted on glass slides with ProLong Diamond Antifade Reagent (P36965; Thermo Fisher Scientific, Waltham, MA, USA). Mountant was allowed to cure for at least 24 h before storage at 4°C or imaging. In a subset of PV-Cre mice, in which PV + STN neurons expressed eNpHR3.0-eYFP, adjacent sections of the STN were processed for the immunohistochemical detection of PV, as described above (primary antibody: 1:1000 guinea pig anti-PV; Synaptic Systems; RRID:AB_2156476; secondary antibody: 1:250 Alexa Fluor 594 donkey anti-guinea pig IgG; Jackson ImmunoResearch Laboratories; RRID:AB_2340474). DiI and immunofluorescent labeling were visualized using confocal laser scanning microscopy (A1, A1R or AX R; Nikon Instruments Inc., Melville, NY, USA). Whole-brain confocal images with DiI- or Iba1-labeled electrode tracks were plotted in the Allen Institute Common Coordinate Framework (CCF) using NeuroInfo

(MBF Bioscience, Williston, VT, USA). Immunohistochemical and confocal imaging procedures are also available at: https://doi.org/10.17504/protocols.io.14egn2xrpg5d/v1 and https://doi.org/10.17504/protocols.io.rm7vzbn9rvx1/v1, respectively.

QUANTIFICATION AND STATISTICAL ANALYSIS

Treadmill behavior—Head-fixed mice spontaneously transitioned between periods of rest and locomotion. A treadmill velocity ≥0.25 cm/s for ≥200 ms was defined as locomotion. The start of a locomotor bout was defined as the first time point that treadmill velocity reached or exceeded 0.25 cm/s. The end of a locomotor bout was defined as the first time point that treadmill velocity fell below 0.25 cm/s for ≥500 ms. For electrophysiological comparisons, the minimum duration of a locomotor bout was defined as ≥ 1 s to prevent inclusion of short duration or fractionated running. Epochs during which locomotion occurred were divided into discrete periods defined as “rest” (1–2 s before locomotion onset), “pre-locomotion” (1 s before locomotion onset), “locomotion” (duration of the locomotor bout, as defined above), “post-locomotion” (1 s after locomotion), and “rest” (1–2 s after locomotion). To allow full sampling of the rest and peri-locomotor periods defined above, only locomotor bouts that were separated by > 3 s were analyzed. 30 s periods of continuous rest were used to analyze baseline neuronal activity. To compare locomotion parameters in WT and Q175 mice, 25 randomly selected bouts from each mouse were analyzed. Locomotor velocity was calculated by measuring the average treadmill velocity over each locomotor bout. Locomotor bout duration was determined by measuring the time from initiation to termination of locomotion, as defined above. The effects of optogenetic inhibition of the STN were studied in mice at rest or during coincident self-initiated locomotion. The impact of optogenetic inhibition on coincident locomotion was measured from the start of optogenetic inhibition to the end of the locomotor bout.

DeepLabCut (version 2.2.2) was used to track the movement of the contralateral forepaw and hindpaw during locomotion. To create the training set, the hindpaw and forepaw were labeled in 20 frames from each of 48 videos (960 total frames) in 6 mice. 95% of the labeled data was used for training and 5% of labeled data was held out for testing. A ResNet-50-based neural network with an imgaug data loader for 500,000 training iterations was used for training. The test error was: 2.61 pixels, train: 3.71 pixels (image size was 720 × 540 pixels). We then used a p-cutoff of 0.9 to condition the X, Y coordinates for future analysis. The network was then used to analyze videos across similar experimental settings. The x axis displacement of the hind paw was used to track the locomotor cycle. The valley and peak within each successive cycle were determined and used to classify the stance/propulsive phase (valley to peak) and swing phase (peak to valley). For outcome measures we compared the time, length, and velocity of the stance and swing phases during locomotion. To compare the kinematics of locomotion in Q175 and WT mice locomotor bouts that were sustained and equivalent in duration (3–5 s) were analyzed. There was no significant difference in the duration of the locomotor bouts used for this analysis (WT: 3.9, 3.5–4.5 s, $n = 61$ bouts; Q175: 3.7, 3.4–4.3 s, $n = 70$ bouts; values represent median and interquartile range). For optogenetic experiments, the impact of optogenetic inhibition on paw kinematics during coincident locomotion was analyzed by comparing equivalent numbers of step cycles in the pre-stimulus and optogenetic inhibition periods.

***In vivo* electrophysiological analysis—**Putative single-unit activity was discriminated with Plexon Offline Sorter software (Plexon, Inc., Dallas, Texas, USA; RRID:SCR_000012) using a combination of template matching, principal component analysis, and manual clustering. For classification of a single unit, sorting had to meet the following inclusion criteria: (1) PCA clusters were significantly different ($p < 0.05$); (2) J3-statistic ≥1; (3) Davies Bouldin test statistic ≤0.5. In addition, a threshold of <0.5% of interspike intervals under 2 ms was required for classification as a putative single unit (% interspike interval within 2 ms; WT: 0.074, 0.0–0.200, $n = 99$; Q175: 0.0, 0.0–0.117, $n = 103$; values represent median and interquartile range). Electrophysiological data were visually inspected in NeuroExplorer (Nex Technologies; RRID:SCR_001818) and then exported to MATLAB (MathWorks, Natick, MA, USA; RRID:SCR_001622) and Mathematica (Wolfram Mathematica; RRID:SCR_014448). Recording sessions with stable unit isolation for ≥2 min were selected for analysis. Mean firing rates were calculated as the reciprocal of the mean interspike interval (1/mean interspike interval). For periods with ≤1 interspike interval (ISI), mean firing rates were calculated as the number of spikes divided by epoch length. The coefficient of variation (CV) of the interspike interval was used as a metric of regularity. If there were less than 3 spikes, the CV could not be calculated and was not reported. Histograms of spike rates (bin = 50 ms) were calculated for the entire recording period. Locomotion, peri-locomotion, and rest periods were defined as described above. Z scores were determined relative to rest using:

bin Z score = (bin spike count –mean spike bin count at rest)/SD of bin counts at rest.

For all locomotor bouts that met the criteria defined above, firing metrics were calculated and then averaged across bouts for each individual neuron. For correlation analysis, the velocity (v(t)) signal from the treadmill encoder was cross-correlated (c(k)) with the smoothed firing rate (r(t)) estimate of STN single units using:

$$c(k) = \sum n - k_{t=1}(r_{t+k} - <r>)(v_t - <v>)/\left(\sum (r_t - <r>)^2 \sum (v_t - <v>)^2\right) \text{ for } k \geq 0$$

$$c(k) = \sum n + k_{t=1}(v_{t-k} - <v>)(r_t - <r>)/\left(\sum (r_t - <r>)^2 \sum (v_t - <v>)^2\right) \text{ for } k < 0$$

The firing rate, r(t), was estimated by smoothing the spike train, s(t), with a Gaussian function (SD = 0.04 s), G(t). Note that at zero lag (i.e., k = 0) this corresponds to Pearson's correlation value. To determine the significance of the cross-correlation measurements, a spike-shuffled dataset was created using the spike times measured from recorded STN units. For each unit, a random draw from its ISI distribution was sampled without replacement using Mathematica's function, RandomChoice[], and added to the first spike time to create the second spike time. Subsequently, another ISI was randomly drawn without replacement and added to the second spike time to create the third spike time, etc. This meant that the first spike time in the shuffled spike trains was always the same, but that subsequent addition of random draws from the ISI distribution created a random sequence of spike times. For each neuron, 20 shuffled spike trains were created, and each was cross-correlated

with the smoothed velocity signal (Gaussian function (SD = 0.012 s)). Peak correlation values were measured and classified as significant if they fell outside of +/− 2 SDs from the average shuffled correlations. For functional classification of STN neurons, units were classified as “type 1,” “type 2,” or “uncorrelated”. Type 1 neurons had to exhibit both (1) a significant positive peak correlation and (2) a positive locomotion-associated Z score. Type 2 neurons had to exhibit both (1) a significant negative peak correlation and (2) a negative locomotion-associated Z score. If neurons failed to meet either of these conditions, they were categorized as uncorrelated.

To examine the relationship between neuronal firing and kinematics, phase histograms were generated in MATLAB. The instantaneous phase of each step cycle was calculated, and each spike was assigned to a phase of the step cycle from 0% to 100% (with 0% and 100% corresponding to the start and end of each cycle, respectively). Spikes phases were measured across cycles from each locomotor epoch and phase histograms were constructed using 10% bins. Spike times from each locomotor epoch were shuffled 1000 times and phase histograms were generated using the shuffled dataset. Neurons were considered phase-locked if their activity exceeded the shuffled mean by 2 SDs.

To determine whether neurons were responsive to optogenetic manipulation, peristimulus time histograms (PSTHs) were constructed from either 4 trials of eNpHR3.0-eYFP stimulation or 50 trials of hChR2(H134R)-eYFP stimulation. vGluT2-and PV-expressing STN neurons were considered directly responsive if their activity fell below 2 SDs of the pre-stimulus mean (5 s preceding stimulus onset) within 100 ms of eNpHR3.0-eYFP stimulation (bin size 100 ms) and/or if spiking was silent throughout the 5 s stimulation period. PV + STN neurons were considered directly responsive if their activity exceeded the pre-stimulus mean (100 ms preceding stimulus onset) by 2 SDs within 10 ms (bin size 1 ms) of hChR2(H134R)-eYFP stimulation.

Experimental design—Data are reported as median and interquartile range in Tables S1–S8. The number and nature of observations for each parameter are specified in Tables S1–S8. Data are represented graphically as violin (kernel density) plots and overlaid boxplots, with the median (central line), interquartile range (box), and 10%–90% range (whiskers) denoted. To ensure that the proposed research was adequately powered, sample sizes were estimated using the formulae described by Noether[96] assuming 80% power (i.e., a 20% probability of a Type 2 error) and a two tailed α level of 0.05. For unpaired data (groups X and Y), and probabilities of X > Y (or X < Y) being 0.7, 0.8, and 0.9, the estimated sample sizes for each group are 33, 15, and 9, respectively. For paired data (where Xi and Xj are independent samples from X, reflecting effect size and sign) and the probabilities of Xi + Xj > 0 being 0.7, 0.8, and 0.9, the estimated sample sizes are 66, 30, and 17, respectively. Probabilities between 0.7 and 0.9 are representative of our historical and pilot data. To minimize assumptions concerning the distribution of data, nonparametric, two-tailed statistical comparisons were made using the Mann–Whitney U (MWU) and Wilcoxon signed-rank (WSR) tests for unpaired and paired comparisons, respectively. In addition, Fisher’s exact test was used for contingency analyses. $p < 0.05$ was considered significant. Where appropriate, p values were adjusted for multiple comparisons using the Holm–Bonferroni method. Statistical tests and p values for each comparison are specified

in Tables S1–S8. Plots and statistical comparisons were generated in Prism (GraphPad Software, San Diego, CA, USA; RRID:SCR_002798) and R (https://www.r-project.org/; RRID:SCR_001905).

Supplementary Material

Refer to Web version on PubMed Central for supplementary material.

ACKNOWLEDGMENTS

This work was funded by grants from CHDI Foundation (A-5071), Aligning Science Across Parkinson's (ASAP-020600), and NIH-NINDS (R01 NS041280 and R01 NS121174). The authors thank Sasha Ulrich, Danielle Rae Schowalter, and Marisha Alicea for maintenance of mouse colonies and Drs. Vahri Beaumont, Roger Cachope, and Ignacio Munoz-Sanjuan for helpful discussions and advice throughout the execution of this study.

REFERENCES

1. Klaus A, Alves da Silva J, and Costa RM (2019). What, If, and When to Move: Basal Ganglia Circuits and Self-Paced Action Initiation. Annu. Rev. Neurosci. 42, 459–483. 10.1146/annurev-neuro-072116-031033. [PubMed: 31018098]
2. Albin RL, Young AB, and Penney JB (1989). The functional anatomy of basal ganglia disorders. Trends Neurosci. 12, 366–375. 10.1016/0166-2236(89)90074-x. [PubMed: 2479133]
3. Hannah R, and Aron AR (2021). Towards real-world generalizability of a circuit for action-stopping. Nat. Rev. Neurosci. 22, 538–552. 10.1038/s41583-021-00485-1. [PubMed: 34326532]
4. Mink JW, and Thach WT (1993). Basal ganglia intrinsic circuits and their role in behavior. Curr. Opin. Neurobiol. 3, 950–957. 10.1016/0959-4388(93)90167-w. [PubMed: 8124079]
5. Baunez C, Nieoullon A, and Amalric M (1995). In a rat model of parkinsonism, lesions of the subthalamic nucleus reverse increases of reaction time but induce a dramatic premature responding deficit. J. Neurosci. 15, 6531–6541. 10.1523/JNEUROSCI.15-10-06531.1995. [PubMed: 7472415]
6. Schmidt R, Leventhal DK, Mallet N, Chen F, and Berke JD (2013). Canceling actions involves a race between basal ganglia pathways. Nat. Neurosci. 16, 1118–1124. 10.1038/nn.3456. [PubMed: 23852117]
7. Fife KH, Gutierrez-Reed NA, Zell V, Bailly J, Lewis CM, Aron AR, and Hnasko TS (2017). Causal role for the subthalamic nucleus in interrupting behavior. Elife 6, e27689. 10.7554/eLife.27689. [PubMed: 28742497]
8. Pasquereau B, and Turner RS (2017). A selective role for ventromedial subthalamic nucleus in inhibitory control. Elife 6, e31627. 10.7554/eLife.31627. [PubMed: 29199955]
9. Li B, Nguyen TP, Ma C, and Dan Y (2020). Inhibition of impulsive action by projection-defined prefrontal pyramidal neurons. Proc. Natl. Acad. Sci. USA 117, 17278–17287. 10.1073/pnas.2000523117. [PubMed: 32631999]
10. Mosher CP, Mamelak AN, Malekmohammadi M, Pouratian N, and Rutishauser U (2021). Distinct roles of dorsal and ventral subthalamic neurons in action selection and cancellation. Neuron 109, 869–881.e6. 10.1016/j.neuron.2020.12.025. [PubMed: 33482087]
11. Adam EM, Johns T, and Sur M (2022). Dynamic control of visually guided locomotion through corticosubthalamic projections. Cell Rep. 40, 111139. 10.1016/j.celrep.2022.111139. [PubMed: 35905719]
12. Isoda M, and Hikosaka O (2008). Role for subthalamic nucleus neurons in switching from automatic to controlled eye movement. J. Neurosci. 28, 7209–7218. 10.1523/JNEUROSCI.0487-08.2008. [PubMed: 18614691]
13. Hasegawa T, Chiken S, Kobayashi K, and Nambu A (2022). Subthalamic nucleus stabilizes movements by reducing neural spike variability in monkey basal ganglia. Nat. Commun. 13, 2233. 10.1038/s41467-022-29750-2. [PubMed: 35468893]

14. Polyakova Z, Hatanaka N, Chiken S, and Nambu A (2024). Subthalamic Activity for Motor Execution and Cancelation in Monkeys. J. Neurosci. 44, e1911222024. 10.1523/JNEUROSCI.1911-22.2024. [PubMed: 38290848]
15. Karachi C, Grabli D, Baup N, Mounayar S, Tandé D, François C, and Hirsch EC (2009). Dysfunction of the subthalamic nucleus induces behavioral and movement disorders in monkeys. Mov. Disord. 24, 1183–1192. 10.1002/mds.22547. [PubMed: 19412950]
16. Baron MS, Wichmann T, Ma D, and DeLong MR (2002). Effects of transient focal inactivation of the basal ganglia in parkinsonian primates. J. Neurosci. 22, 592–599. 10.1523/JNEUROSCI.22-02-00592.2002. [PubMed: 11784807]
17. Guillaumin A, Serra GP, Georges F, and Wallén-Mackenzie Å (2021). Experimental investigation into the role of the subthalamic nucleus (STN) in motor control using optogenetics in mice. Brain Res. 1755, 147226. 10.1016/j.brainres.2020.147226. [PubMed: 33358727]
18. Hamada I, and DeLong MR (1992). Excitotoxic acid lesions of the primate subthalamic nucleus result in transient dyskinesias of the contralateral limbs. J. Neurophysiol. 68, 1850–1858. 10.1152/jn.1992.68.5.1850. [PubMed: 1479448]
19. Parolari L, Schneeberger M, Heintz N, and Friedman JM (2021). Functional analysis of distinct populations of subthalamic nucleus neurons on Parkinson's disease and OCD-like behaviors in mice. Mol. Psychiatr. 26, 7029–7046. 10.1038/s41380-021-01162-6.
20. Friedman AD, and Yin HH (2023). Selective Activation of Subthalamic Nucleus Output Quantitatively Scales Movements. J. Neurosci. 43, 7967–7981. 10.1523/JNEUROSCI.0734-23.2023. [PubMed: 37816600]
21. Fan J-P, Zhang X, Han Y, Ji Y, Gu W-X, Wu H-C, Zhou C, and Xiao C (2023). Subthalamic neurons interact with nigral dopaminergic neurons to regulate movement in mice. Acta Physiol. 237, e13917. 10.1111/apha.13917.
22. Schor JS, Gonzalez Montalvo I, Spratt PWE, Brakaj RJ, Stansil JA, Twedell EL, Bender KJ, and Nelson AB (2022). Therapeutic deep brain stimulation disrupts movement-related subthalamic nucleus activity in parkinsonian mice. Elife 11, e75253. 10.7554/eLife.75253. [PubMed: 35786442]
23. Iwamuro H, Tachibana Y, Ugawa Y, Saito N, and Nambu A (2017). Information processing from the motor cortices to the subthalamic nucleus and globus pallidus and their somatotopic organizations revealed electrophysiologically in monkeys. Eur. J. Neurosci. 46, 2684–2701. 10.1111/ejn.13738. [PubMed: 29044874]
24. Wichmann T, Bergman H, and DeLong MR (1994). The primate subthalamic nucleus. I. Functional properties in intact animals. J. Neurophysiol. 72, 494–506. 10.1152/jn.1994.72.2.494. [PubMed: 7983514]
25. Deffains M, Iskhakova L, Katabi S, Haber SN, Israel Z, and Bergman H (2016). Subthalamic, not striatal, activity correlates with basal ganglia downstream activity in normal and parkinsonian monkeys. Elife 5, e16443. 10.7554/eLife.16443. [PubMed: 27552049]
26. Georgopoulos AP, DeLong MR, and Crutcher MD (1983). Relations between parameters of step-tracking movements and single cell discharge in the globus pallidus and subthalamic nucleus of the behaving monkey. J. Neurosci. 3, 1586–1598. 10.1523/JNEUROSCI.03-08-01586.1983. [PubMed: 6875658]
27. DeLong MR (1990). Primate models of movement disorders of basal ganglia origin. Trends Neurosci. 13, 281–285. 10.1016/0166-2236(90)90110-v. [PubMed: 1695404]
28. Fischer P, He S, de Roquemaurel A, Akram H, Foltynie T, Limousin P, Zrinzo L, Hyam J, Cagnan H, Brown P, and Tan H (2020). Entraining Stepping Movements of Parkinson's Patients to Alternating Subthalamic Nucleus Deep Brain Stimulation. J. Neurosci. 40, 8964–8972. 10.1523/JNEUROSCI.1767-20.2020. [PubMed: 33087473]
29. Gulberti A, Wagner JR, Horn MA, Reuss JH, Heise M, Koeppen JA, Pinnschmidt HO, Westphal M, Engel AK, Gerloff C, et al. (2023). Subthalamic and nigral neurons are differentially modulated during parkinsonian gait. Brain 146, 2766–2779. 10.1093/brain/awad006. [PubMed: 36730026]
30. Thenaisie Y, Lee K, Moerman C, Scafa S, Gálvez A, Pirondini E, Burri M, Ravier J, Puiatti A, Accolla E, et al. (2022). Principles of gait encoding in the subthalamic nucleus of people with

Parkinson's disease. Sci. Transl. Med. 14, eabo1800. 10.1126/scitranslmed.abo1800. [PubMed: 36070366]

31. Nambu A (2011). Somatotopic organization of the primate Basal Ganglia. Front. Neuroanat. 5, 26. 10.3389/fnana.2011.00026. [PubMed: 21541304]
32. Jeon H, Lee H, Kwon D-H, Kim J, Tanaka-Yamamoto K, Yook JS, Feng L, Park HR, Lim YH, Cho Z-H, et al. (2022). Topographic connectivity and cellular profiling reveal detailed input pathways and functionally distinct cell types in the subthalamic nucleus. Cell Rep. 38, 110439. 10.1016/j.celrep.2022.110439. [PubMed: 35235786]
33. Kita T, Osten P, and Kita H (2014). Rat subthalamic nucleus and zona incerta share extensively overlapped representations of cortical functional territories. J. Comp. Neurol. 522, 4043–4056. 10.1002/cne.23655. [PubMed: 25048050]
34. DeLong MR, Crutcher MD, and Georgopoulos AP (1985). Primate globus pallidus and subthalamic nucleus: functional organization. J. Neurophysiol. 53, 530–543. 10.1152/jn.1985.53.2.530. [PubMed: 3981228]
35. Afsharpour S (1985). Topographical projections of the cerebral cortex to the subthalamic nucleus. J. Comp. Neurol. 236, 14–28. 10.1002/cne.902360103. [PubMed: 2414329]
36. Haynes WIA, and Haber SN (2013). The organization of prefrontal-subthalamic inputs in primates provides an anatomical substrate for both functional specificity and integration: implications for Basal Ganglia models and deep brain stimulation. J. Neurosci. 33, 4804–4814. 10.1523/JNEUROSCI.4674-12.2013. [PubMed: 23486951]
37. Rodriguez-Rojas R, Pineda-Pardo JA, Mañez-Miro J, Sanchez-Turel A, Martinez-Fernandez R, Del Alamo M, DeLong M, and Obeso JA (2022). Functional Topography of the Human Subthalamic Nucleus: Relevance for Subthalamotomy in Parkinson's Disease. Mov. Disord. 37, 279–290. 10.1002/mds.28862. [PubMed: 34859498]
38. Kolomiets BP, Deniau JM, Mailly P, Ménétrey A, Glowinski J, and Thierry AM (2001). Segregation and Convergence of Information Flow through the Cortico-Subthalamic Pathways. J. Neurosci. 21, 5764–5772. 10.1523/JNEUROSCI.21-15-05764.2001. [PubMed: 11466448]
39. Maurice N, Deniau JM, Glowinski J, and Thierry AM (1998). Relationships between the prefrontal cortex and the basal ganglia in the rat: physiology of the corticosubthalamic circuits. J. Neurosci. 18, 9539–9546. 10.1523/JNEUROSCI.18-22-09539.1998. [PubMed: 9801390]
40. Wan XST, Liang F, Moret V, Wieesendanger M, and Rouiller EM (1992). Mapping of the motor pathways in rats: c-fos induction by intracortical microstimulation of the motor cortex correlated with efferent connectivity of the site of cortical stimulation. Neuroscience 49, 749–761. 10.1016/0306-4522(92)90353-4. [PubMed: 1279454]
41. Muñoz-Castañeda R, Zingg B, Matho KS, Chen X, Wang Q, Foster NN, Li A, Narasimhan A, Hirokawa KE, Huo B, et al. (2021). Cellular anatomy of the mouse primary motor cortex. Nature 598, 159–166. 10.1038/s41586-021-03970-w. [PubMed: 34616071]
42. Wessel JR, and Aron AR (2017). On the Globality of Motor Suppression: Unexpected Events and Their Influence on Behavior and Cognition. Neuron 93, 259–280. 10.1016/j.neuron.2016.12.013. [PubMed: 28103476]
43. Bevan MD, Clarke NP, and Bolam JP (1997). Synaptic integration of functionally diverse pallidal information in the entopeduncular nucleus and subthalamic nucleus in the rat. J. Neurosci. 17, 308–324. 10.1523/JNEUROSCI.17-01-00308.1997. [PubMed: 8987757]
44. Wallén-Mackenzie Å, Dumas S, Papathanou M, Martis Thiele MM, Vlcek B, König N, and Björklund ÅK (2020). Spatio-molecular domains identified in the mouse subthalamic nucleus and neighboring glutamatergic and GABAergic brain structures. Commun. Biol. 3, 338. 10.1038/s42003-020-1028-8. [PubMed: 32620779]
45. Parent A, Fortin M, Côté PY, and Cicchetti F (1996). Calcium-binding proteins in primate basal ganglia. Neurosci. Res. 25, 309–334. 10.1016/0168-0102(96)01065-6. [PubMed: 8866512]
46. Zhang Y, Roy DS, Zhu Y, Chen Y, Aida T, Hou Y, Shen C, Lea NE, Schroeder ME, Skaggs KM, et al. (2022). Targeting thalamic circuits rescues motor and mood deficits in PD mice. Nature 607, 321–329. 10.1038/s41586-022-04806-x. [PubMed: 35676479]

47. Blumenfeld Z, and Brontë-Stewart H (2015). High Frequency Deep Brain Stimulation and Neural Rhythms in Parkinson's Disease. Neuropsychol. Rev. 25, 384–397. 10.1007/s11065-015-9308-7. [PubMed: 26608605]
48. Vitek JL, and Giroux M (2000). Physiology of hypokinetic and hyperkinetic movement disorders: model for dyskinesia. Ann. Neurol. 47, S131–S140. [PubMed: 10762140]
49. Hammond C, Bergman H, and Brown P (2007). Pathological synchronization in Parkinson's disease: networks, models and treatments. Trends Neurosci. 30, 357–364. 10.1016/j.tins.2007.05.004. [PubMed: 17532060]
50. Callahan JW, Wokosin DL, and Bevan MD (2022). Dysregulation of the Basal Ganglia Indirect Pathway in Early Symptomatic Q175 Huntington's Disease Mice. J. Neurosci. 42, 2080–2102. 10.1523/JNEUROSCI.0782-21.2022. [PubMed: 35058372]
51. Beaumont V, Zhong S, Lin H, Xu W, Bradaia A, Steidl E, Gleyzes M, Wadel K, Buisson B, Padovan-Neto FE, et al. (2016). Phosphodiesterase 10A Inhibition Improves Cortico-Basal Ganglia Function in Huntington's Disease Models. Neuron 92, 1220–1237. 10.1016/j.neuron.2016.10.064. [PubMed: 27916455]
52. Atherton JF, McIver EL, Mullen MR, Wokosin DL, Surmeier DJ, and Bevan MD (2016). Early dysfunction and progressive degeneration of the subthalamic nucleus in mouse models of Huntington's disease. Elife 5, e21616. 10.7554/eLife.21616. [PubMed: 27995895]
53. Vitek JL, Patriat R, Ingham L, Reich MM, Volkmann J, and Harel N (2022). Lead location as a determinant of motor benefit in subthalamic nucleus deep brain stimulation for Parkinson's disease. Front. Neurosci. 16, 1010253. 10.3389/fnins.2022.1010253. [PubMed: 36267235]
54. Zaidel A, Spivak A, Grieb B, Bergman H, and Israel Z (2010). Subthalamic span of beta oscillations predicts deep brain stimulation efficacy for patients with Parkinson's disease. Brain 133, 2007–2021. 10.1093/brain/awq144. [PubMed: 20534648]
55. Chabardes S, Krack P, Piallat B, Bougerol T, Seigneuret E, Yelnik J, Fernandez Vidal S, David O, Mallet L, Benabid A-L, and Polosan M (2020). Deep brain stimulation of the subthalamic nucleus in obsessive-compulsives disorders: long-term follow-up of an open, prospective, observational cohort. J. Neurol. Neurosurg. Psychiatry 91, 1349–1356. 10.1136/jnnp-2020-323421. [PubMed: 33033168]
56. Huang Y, Aronson JP, Pilitsis JG, Gee L, Durphy J, Molho ES, and Ramirez-Zamora A (2018). Anatomical Correlates of Uncontrollable Laughter With Unilateral Subthalamic Deep Brain Stimulation in Parkinson's Disease. Front. Neurol. 9, 341. 10.3389/fneur.2018.00341. [PubMed: 29887826]
57. Accolla EA, Herrojo Ruiz M, Horn A, Schneider G-H, Schmitz-Hübsch T, Draganski B, and Kühn AA (2016). Brain networks modulated by subthalamic nucleus deep brain stimulation. Brain 139, 2503–2515. 10.1093/brain/aww182. [PubMed: 27412387]
58. Koch ET, Sepers MD, Cheng J, and Raymond LA (2022). Early Changes in Striatal Activity and Motor Kinematics in a Huntington's Disease Mouse Model. Mov. Disord. 37, 2021–2032. 10.1002/mds.29168. [PubMed: 35880748]
59. Heikkinen T, Bragge T, Bhattarai N, Parkkari T, Puoliväli J, Kontkanen O, Sweeney P, Park LC, and Munoz-Sanjuan I (2020). Rapid and robust patterns of spontaneous locomotor deficits in mouse models of Huntington's disease. PLoS One 15, e0243052. 10.1371/journal.pone.0243052. [PubMed: 33370315]
60. Menalled LB, Kudwa AE, Miller S, Fitzpatrick J, Watson-Johnson J, Keating N, Ruiz M, Mushlin R, Alosio W, McConnell K, et al. (2012). Comprehensive behavioral and molecular characterization of a new knock-in mouse model of Huntington's disease: zQ175. PLoS One 7, e49838. 10.1371/journal.pone.0049838. [PubMed: 23284626]
61. Heikkinen T, Lehtimäki K, Vartiainen N, Puoliväli J, Hendricks SJ, Glaser JR, Bradaia A, Wadel K, Touller C, Kontkanen O, et al. (2012). Characterization of neurophysiological and behavioral changes, MRI brain volumetry and 1H MRS in zQ175 knock-in mouse model of Huntington's disease. PLoS One 7, e50717. 10.1371/journal.pone.0050717. [PubMed: 23284644]
62. Lange H, Thörner G, Hopf A, and Schröder KF (1976). Morphometric studies of the neuropathological changes in choreatic diseases. J. Neurol. Sci. 28, 401–425. 10.1016/0022-510x(76)90114-3. [PubMed: 133209]

63. Nath T, Mathis A, Chen AC, Patel A, Bethge M, and Mathis MW (2019). Using DeepLabCut for 3D markerless pose estimation across species and behaviors. Nat. Protoc. 14, 2152–2176. 10.1038/s41596-019-0176-0. [PubMed: 31227823]
64. Mathis A, Mamidanna P, Cury KM, Abe T, Murthy VN, Mathis MW, and Bethge M (2018). DeepLabCut: markerless pose estimation of user-defined body parts with deep learning. Nat. Neurosci. 21, 1281–1289. 10.1038/s41593-018-0209-y. [PubMed: 30127430]
65. Hallworth NE, and Bevan MD (2005). Globus Pallidus Neurons Dynamically Regulate the Activity Pattern of Subthalamic Nucleus Neurons through the Frequency-Dependent Activation of Postsynaptic GABA $_A$ and GABA $_B$ Receptors. J. Neurosci. 25, 6304–6315. 10.1523/JNEUROSCI.0450-05.2005. [PubMed: 16000620]
66. Bevan MD, Magill PJ, Hallworth NE, Bolam JP, and Wilson CJ (2002). Regulation of the Timing and Pattern of Action Potential Generation in Rat Subthalamic Neurons In Vitro by GABA-A IPSPs. J. Neurophysiol. 87, 1348–1362. 10.1152/jn.00582.2001. [PubMed: 11877509]
67. Musall S, Kaufman MT, Juavinett AL, Gluf S, and Churchland AK (2019). Single-trial neural dynamics are dominated by richly varied movements. Nat. Neurosci. 22, 1677–1686. 10.1038/s41593-019-0502-4. [PubMed: 31551604]
68. Bevan MD, and Bolam JP (1995). Cholinergic, GABAergic, and glutamate-enriched inputs from the mesopontine tegmentum to the subthalamic nucleus in the rat. J. Neurosci. 15, 7105–7120. 10.1523/JNEUROSCI.15-11-07105.1995. [PubMed: 7472465]
69. Bevan MD, Francis CM, and Bolam JP (1995). The glutamate-enriched cortical and thalamic input to neurons in the subthalamic nucleus of the rat: convergence with GABA-positive terminals. J. Comp. Neurol. 361, 491–511. 10.1002/cne.903610312. [PubMed: 8550895]
70. Beloozerova IN, and Marlinski V (2020). Contribution of the ventrolateral thalamus to the locomotion-related activity of motor cortex. J. Neurophysiol. 124, 1480–1504. 10.1152/jn.00253.2020. [PubMed: 32783584]
71. Watson GDR, Hughes RN, Petter EA, Fallon IP, Kim N, Severino FPU, and Yin HH (2021). Thalamic projections to the subthalamic nucleus contribute to movement initiation and rescue of parkinsonian symptoms. Sci. Adv. 7, eabe9192. 10.1126/sciadv.abe9192. [PubMed: 33547085]
72. Kovaleski RF, Callahan JW, Chazalon M, Wokosin DL, Baufreton J, and Bevan MD (2020). Dysregulation of external globus pallidus-subthalamic nucleus network dynamics in parkinsonian mice during cortical slow-wave activity and activation. J. Physiol. 598, 1897–1927. 10.1113/JP279232. [PubMed: 32112413]
73. Dodson PD, Larvin JT, Duffell JM, Garas FN, Doig NM, Kessaris N, Duguid IC, Bogacz R, Butt SJB, and Magill PJ (2015). Distinct developmental origins manifest in the specialized encoding of movement by adult neurons of the external globus pallidus. Neuron 86, 501–513. 10.1016/j.neuron.2015.03.007. [PubMed: 25843402]
74. Aristieta A, Barresi M, Azizpour Lindi S, Barrière G, Courtand G, de la Crompe B, Guilhemsang L, Gauthier S, Fioramonti S, Baufreton J, and Mallet NP (2021). A Disynaptic Circuit in the Globus Pallidus Controls Locomotion Inhibition. Curr. Biol. 31, 707–721.e7. 10.1016/j.cub.2020.11.019. [PubMed: 33306949]
75. Ketzef M, and Silberberg G (2021). Differential Synaptic Input to External Globus Pallidus Neuronal Subpopulations In Vivo. Neuron 109, 516–529.e4. 10.1016/j.neuron.2020.11.006. [PubMed: 33248017]
76. Zeng H (2022). What is a cell type and how to define it? Cell 185, 2739–2755. 10.1016/j.cell.2022.06.031. [PubMed: 35868277]
77. Tecuapetla F, Jin X, Lima SQ, and Costa RM (2016). Complementary Contributions of Striatal Projection Pathways to Action Initiation and Execution. Cell 166, 703–715. 10.1016/j.cell.2016.06.032. [PubMed: 27453468]
78. Parker JG, Marshall JD, Ahanonu B, Wu Y-W, Kim TH, Grewe BF, Zhang Y, Li JZ, Ding JB, Ehlers MD, and Schnitzer MJ (2018). Diametric neural ensemble dynamics in parkinsonian and dyskinetic states. Nature 557, 177–182. 10.1038/s41586-018-0090-6. [PubMed: 29720658]
79. Cui G, Jun SB, Jin X, Pham MD, Vogel SS, Lovinger DM, and Costa RM (2013). Concurrent activation of striatal direct and indirect pathways during action initiation. Nature 494, 238–242. 10.1038/nature11846. [PubMed: 23354054]

80. Markowitz JE, Gillis WF, Beron CC, Neufeld SQ, Robertson K, Bhagat ND, Peterson RE, Peterson E, Hyun M, Linderman SW, et al. (2018). The Striatum Organizes 3D Behavior via Moment-to-Moment Action Selection. Cell 174, 44–58.e17. 10.1016/j.cell.2018.04.019. [PubMed: 29779950]
81. Kravitz AV, Freeze BS, Parker PRL, Kay K, Thwin MT, Deisseroth K, and Kreitzer AC (2010). Regulation of parkinsonian motor behaviours by optogenetic control of basal ganglia circuitry. Nature 466, 622–626. 10.1038/nature09159. [PubMed: 20613723]
82. Roseberry TK, Lee AM, Lalive AL, Wilbrecht L, Bonci A, and Kreitzer AC (2016). Cell-Type-Specific Control of Brainstem Locomotor Circuits by Basal Ganglia. Cell 164, 526–537. 10.1016/j.cell.2015.12.037. [PubMed: 26824660]
83. Mizes KGC, Lindsey J, Escola GS, and Ölveczky BP (2023). Dissociating the contributions of sensorimotor striatum to automatic and visually guided motor sequences. Nat. Neurosci. 26, 1791–1804. 10.1038/s41593-023-01431-3. [PubMed: 37667040]
84. Azcorra M, Gaertner Z, Davidson C, He Q, Kim H, Nagappan S, Hayes CK, Ramakrishnan C, Fenno L, Kim YS, et al. (2023). Unique functional responses differentially map onto genetic subtypes of dopamine neurons. Nat. Neurosci. 26, 1762–1774. 10.1038/s41593-023-01401-9. [PubMed: 37537242]
85. Howe MW, and Dombeck DA (2016). Rapid signalling in distinct dopaminergic axons during locomotion and reward. Nature 535, 505–510. 10.1038/nature18942. [PubMed: 27398617]
86. Lahiri AK, and Bevan MD (2020). Dopaminergic Transmission Rapidly and Persistently Enhances Excitability of D1 Receptor-Expressing Striatal Projection Neurons. Neuron 106, 277–290.e6. 10.1016/j.neuron.2020.01.028. [PubMed: 32075716]
87. Markowitz JE, Gillis WF, Jay M, Wood J, Harris RW, Cieszkowski R, Scott R, Brann D, Koveal D, Kula T, et al. (2023). Spontaneous behaviour is structured by reinforcement without explicit reward. Nature 614, 108–117. 10.1038/s41586-022-05611-2. [PubMed: 36653449]
88. da Silva JA, Tecuapetla F, Paixão V, and Costa RM (2018). Dopamine neuron activity before action initiation gates and invigorates future movements. Nature 554, 244–248. 10.1038/nature25457. [PubMed: 29420469]
89. Coddington LT, and Dudman JT (2018). The timing of action determines reward prediction signals in identified midbrain dopamine neurons. Nat. Neurosci. 21, 1563–1573. 10.1038/s41593-018-0245-7. [PubMed: 30323275]
90. Tabrizi SJ, Flower MD, Ross CA, and Wild EJ (2020). Huntington disease: new insights into molecular pathogenesis and therapeutic opportunities. Nat. Rev. Neurol. 16, 529–546. 10.1038/s41582-020-0389-4. [PubMed: 32796930]
91. Cossu G, and Pau M (2017). Subthalamic nucleus stimulation and gait in Parkinson's Disease: a not always fruitful relationship. Gait Posture 52, 205–210. 10.1016/j.gaitpost.2016.11.039. [PubMed: 27915226]
92. Bosley KM, Luo Z, Amoozegar S, Acedillo K, Nakajima K, Johnson LA, Vitek JL, and Wang J (2023). Effect of subthalamic coordinated reset deep brain stimulation on Parkinsonian gait. Front. Neuroinf. 17, 1185723. 10.3389/fninf.2023.1185723.
93. Gradinaru V, Zhang F, Ramakrishnan C, Mattis J, Prakash R, Diester I, Goshen I, Thompson KR, and Deisseroth K (2010). Molecular and cellular approaches for diversifying and extending optogenetics. Cell 141, 154–165. 10.1016/j.cell.2010.02.037. [PubMed: 20303157]
94. Schindelin J, Arganda-Carreras I, Frise E, Kaynig V, Longair M, Pietzsch T, Preibisch S, Rueden C, Saalfeld S, Schmid B, et al. (2012). Fiji: an open-source platform for biological-image analysis. Nat. Methods 9, 676–682. 10.1038/nmeth.2019. [PubMed: 22743772]
95. Dessau RB, and Pipper CB (2008). ["R"–project for statistical computing]. Ugeskr. Laeger 170, 328–330. [PubMed: 18252159]
96. Noether GE (1987). Sample size determination for some common nonparametric tests. Journal of the American Statistical Association. J. Am. Stat. Assoc. 82, 645–647.

Highlights

- The activities of most STN neurons (type 1) increase prior to and during locomotion
- 50% of type 1 neurons discharge most during the propulsive phase of locomotion
- Brief optogenetic inhibition of type 1 activity dysregulates locomotion
- Gait deficits in Huntington's disease mice are associated with type 1 hypoactivity

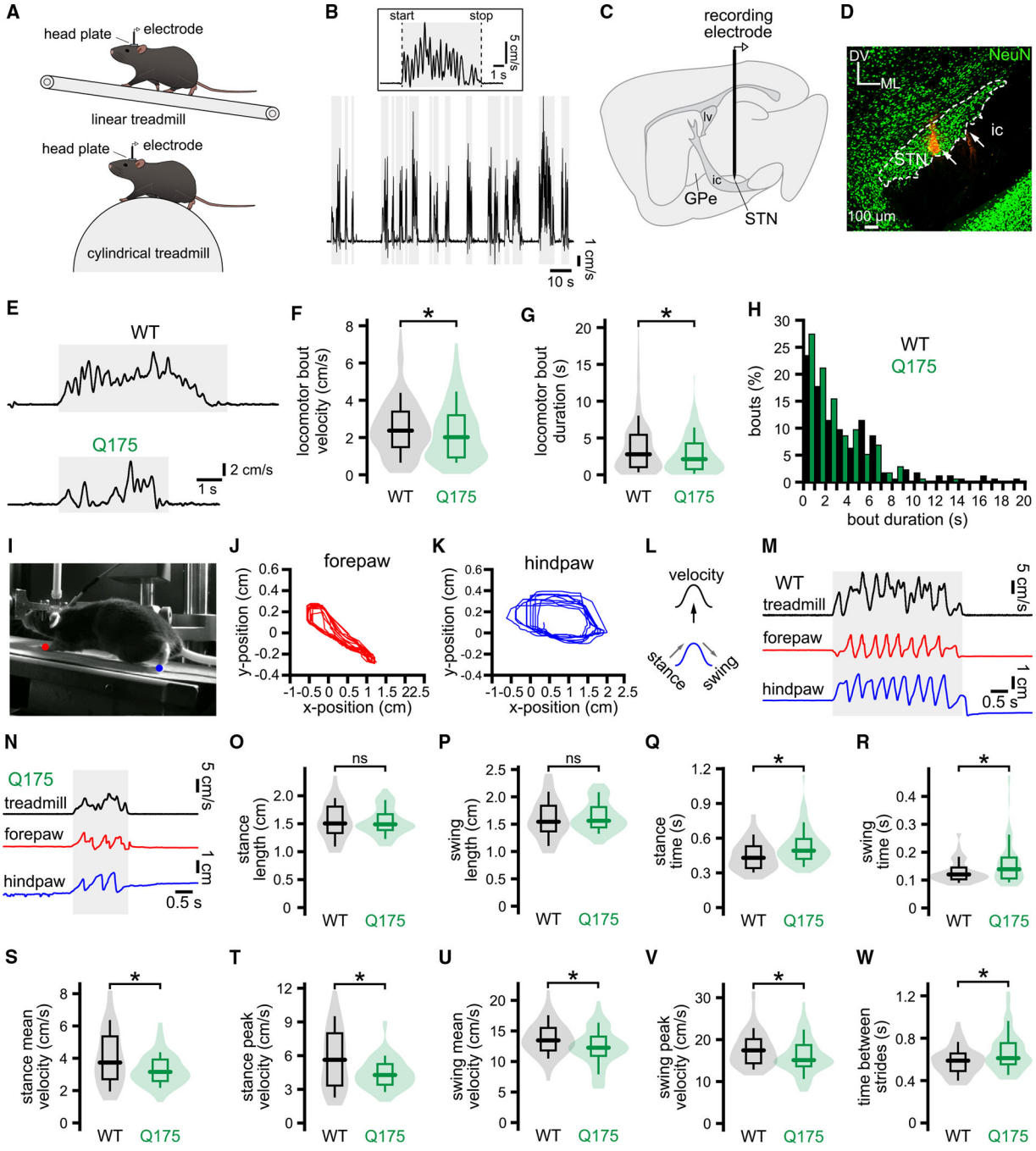

Figure 1. Self-initiated locomotion is dysregulated in Q175 HD mice

(A) STN encoding of self-initiated locomotion was assessed in head-fixed mice that were habituated to a self-paced linear or cylindrical treadmill.

(B) A treadmill velocity encoder was used to detect periods of rest and bouts of self-initiated treadmill locomotion.

(C) STN activity was recorded with a 32- or 64-channel silicon electrode/optrode.

(D) The locations of STN recordings were assessed histologically using DiI red labeling (white arrows) and immunohistochemical detection of NeuN (green). The dorsoventral

(DV) and mediolateral (ML) axes and internal capsule (ic) are denoted. In some cases, immunohistochemical detection of IBA1 was used to locate electrode tracks instead of DiI red (not illustrated).

(E–H) Self-initiated treadmill locomotor bouts were shorter in duration and of lower velocity in Q175 HD mice versus WT mice (E, representative treadmill velocity encoder traces; F–H, population data).

(I–N) DeepLabCut-based analysis of high-frame-rate digital video was used to track 2D contralateral paw movement in the x and y axes during self-initiated locomotion and rest (I, head-fixed mouse on a linear treadmill, with forepaw [red] and hindpaw [blue] tracking denoted; J and K, x-y coordinates of the forepaws [J, red] and hindpaws [K, blue] during locomotion; L–N, schematized [L] and example relationships of treadmill velocity and x axis displacement of the contralateral paws during treadmill locomotion in WT [M] and Q175 [N] mice).

(O–W) X axis kinematics of the contralateral hindpaw in WT and Q175 mice during locomotion. The lengths of the stance and swing phases of locomotion were not significantly different in Q175 and WT mice (O and P). The durations (Q and R) and velocities (S–V) of both the stance and swing phases were longer and lower, respectively, in Q175 versus WT mice. During locomotion, the time between strides was longer in Q175 mice (W). *$p < 0.05$; ns, not significant.

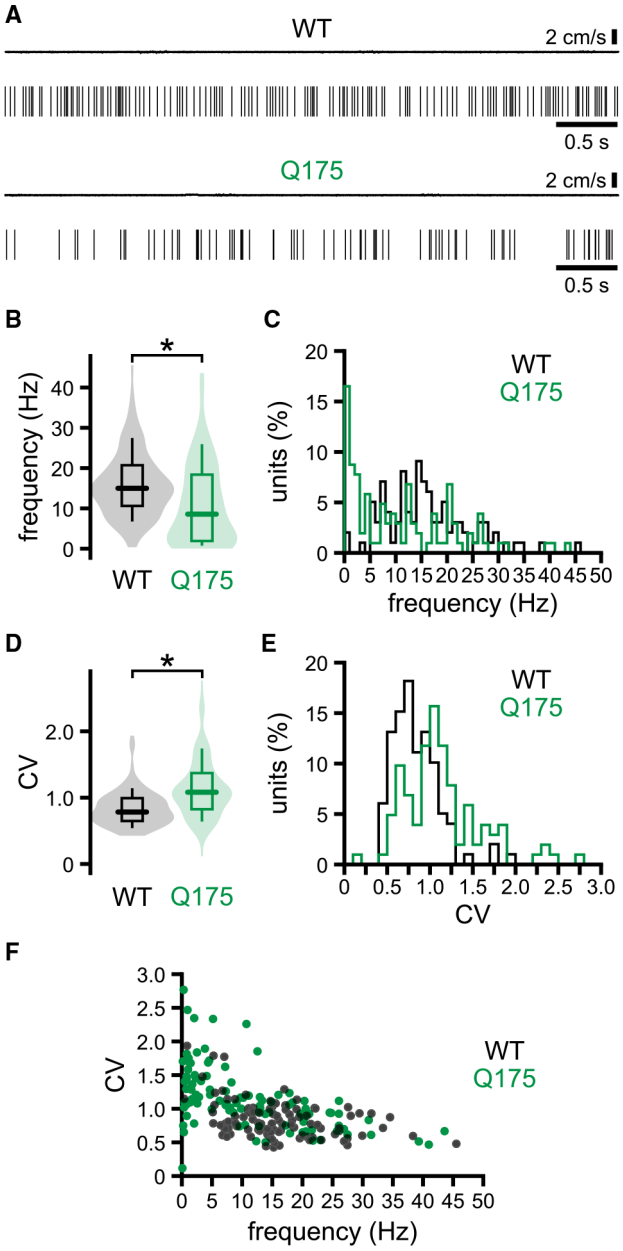

Figure 2. The frequency and precision of STN unit activity are lower in Q175 HD versus WT mice at rest

(A) Representative spike rasters of STN units and associated treadmill velocity encoder records in WT and Q175 mice at rest.

(B–F, population data) The mean frequency and precision (coefficient of variation of the interspike interval, CV) of STN activity are lower in resting Q175 mice compared to WT. *$p < 0.05$.

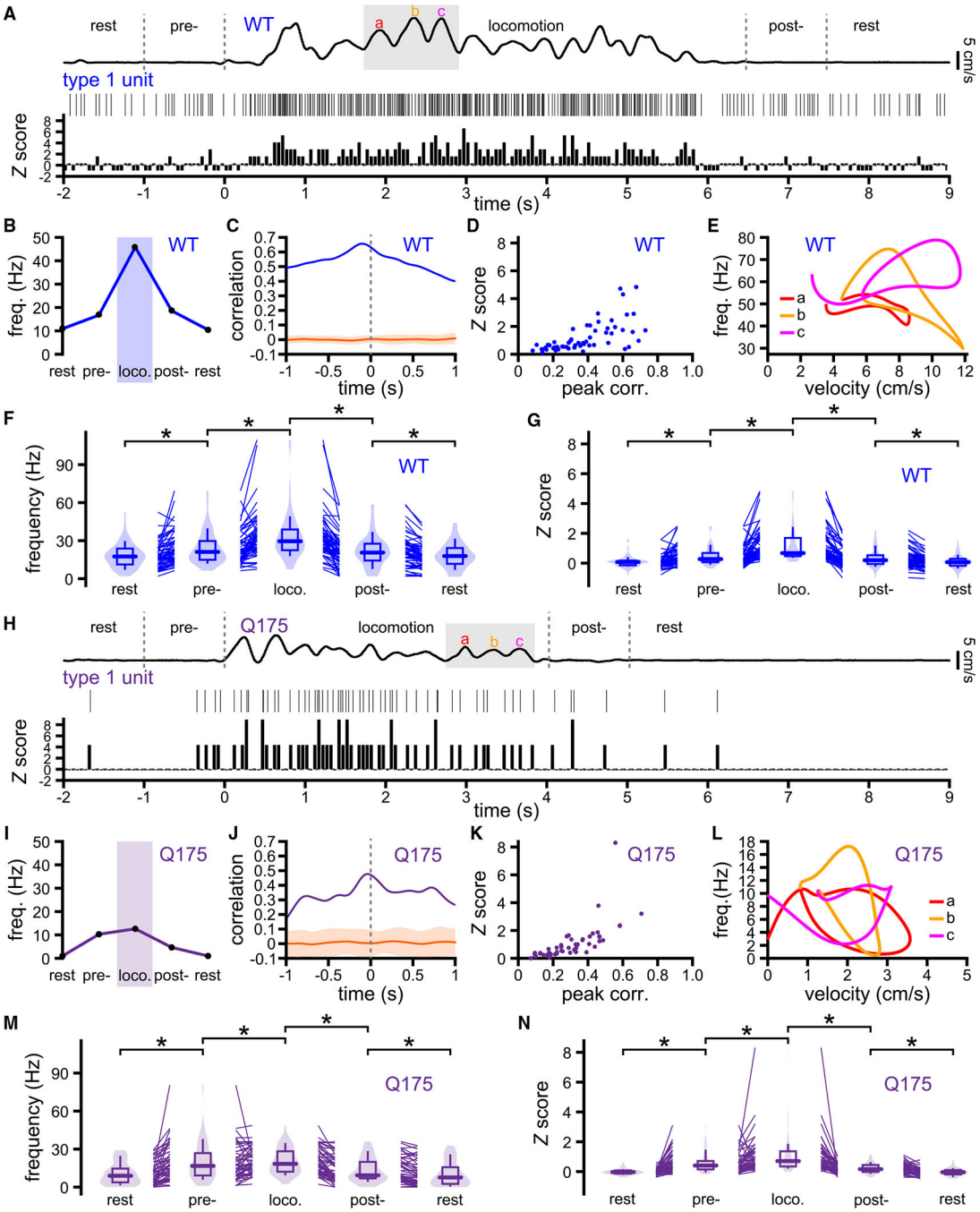

Figure 3. Type 1 STN neurons in WT and Q175 mice exhibit locomotion-associated increases in firing

(A) Locomotion-associated activity of a representative type 1 STN neuron in a WT mouse (upper trace, treadmill velocity; middle trace, spike raster; lower trace, *Z* score of spikes per 50-ms time bin relative to baseline spike counts).

(B) Average firing frequency of the neuron in (A) during the initial rest, pre-locomotion, locomotion, post-locomotion, and subsequent rest periods.

(C) Spike frequency-treadmill velocity correlation (blue) versus the correlation after shuffling (orange, mean ± 2 SD).

(D) Peak correlation versus *Z* score for the sample population.
(E) The spiking rate of the neuron in (A) varied inconsistently over several cycles of velocity change (a, b, and c; color coded as for A).
(F and G) Frequency (F) and *Z* score (G) population data for type 1 neurons in WT mice.
(H) Locomotion-associated activity of a representative type 1 STN neuron in a Q175 mouse (upper trace, treadmill velocity; middle trace, spike raster; lower trace, *Z* score of spikes per 50-ms time bin relative to baseline spike counts).
(I) Average firing frequency of the neuron in (H) during the initial rest, pre-locomotion, locomotion, post-locomotion, and subsequent rest periods.
(J) Spike frequency-treadmill velocity correlation (purple) versus the correlation after shuffling (orange, mean ± 2 SD).
(K) Peak correlation versus *Z* score for the sample population.
(L) The spiking rate of the neuron in (H) varied inconsistently over several cycles of velocity change (a, b, and c; color coded as for H). (M and N) Frequency (M) and *Z* score (N) population data for type 1 neurons in Q175 mice. $*p < 0.05$.

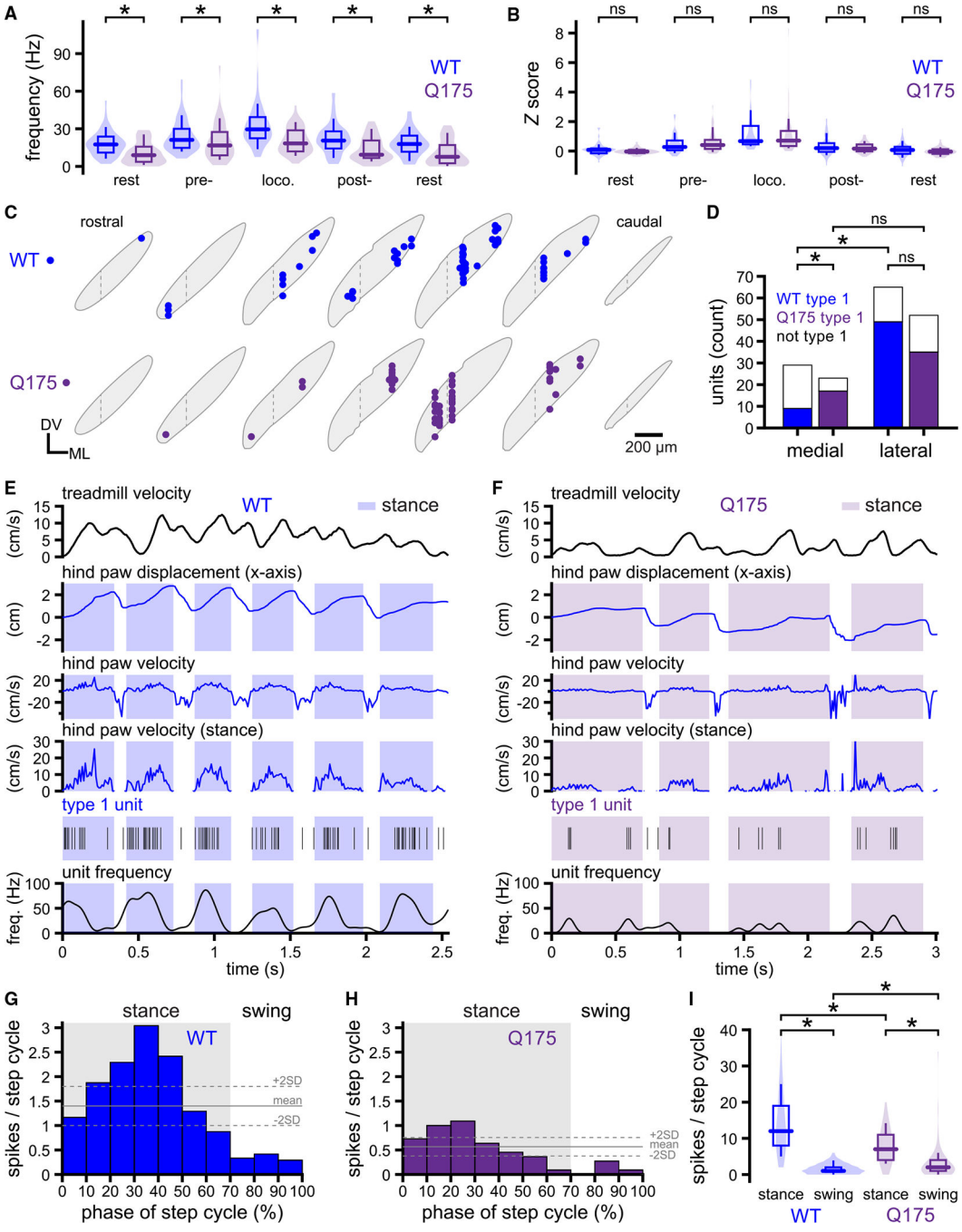

Figure 4. The frequencies of resting and locomotion-associated type 1 STN activity are reduced in Q175 mice

(A and B) Population data. The frequency (A) but not *Z* score (B) of locomotion-associated type 1 STN activity was reduced in Q175 mice.

(C and D) Distribution of recorded type 1 STN neurons in WT and Q175 mice. In WT mice, type 1 units were relatively abundant in the dorsolateral two-thirds of the STN compared to the medial third. In the medial third of the STN, type 1 units were more prevalent in Q175 than WT mice. The boundary between the medial third and lateral two-thirds of the STN is denoted by a dashed line.

(E–I) A subset of type 1 STN neurons in WT and Q175 mice exhibited firing that was related to the phase of the locomotor cycle (E–H, representative examples; I, population data). (I) The number of spikes during the stance phase of the locomotor cycle was significantly lower in Q175 mice.*$p < 0.05$; ns, not significant.

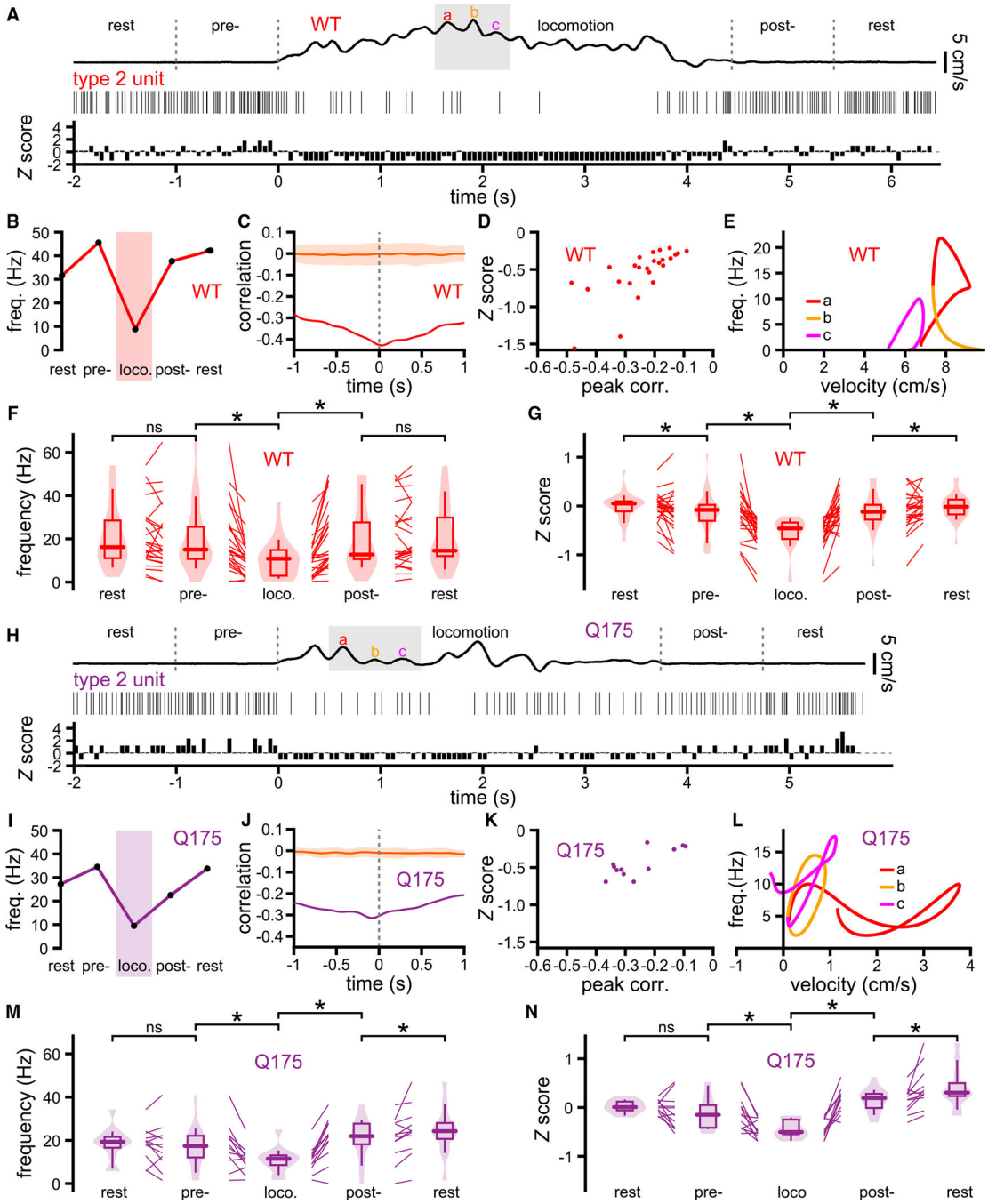

Figure 5. Type 2 STN neurons in WT and Q175 mice exhibit locomotion-associated decreases in firing

(A) Locomotion-associated activity of a representative type 2 STN neuron in a WT mouse (upper trace, treadmill velocity; middle trace, spike raster; lower trace, *Z* score of spikes per 50-ms time bin relative to baseline spike counts).

(B) Average firing frequency of the neuron in (A) during the initial rest, pre-locomotion, locomotion, post-locomotion, and subsequent rest periods.

(C) Spike frequency-treadmill velocity correlation (red) versus the correlation after shuffling (orange, mean ± 2 SD).

(D) Peak correlation versus *Z* score for the sample population.
(E) The spiking rate of the neuron in (A) varied inconsistently over several cycles of velocity change (a, b, and c; color coded as for A).
(F and G) Frequency (F) and *Z* score (G) population data for type 2 neurons in WT mice.
(H) Locomotion-associated activity of a representative type 2 STN neuron in a Q175 mouse (upper trace, treadmill velocity; middle trace, spike raster; lower trace, *Z* score of spikes per 50-ms time bin relative to baseline spike counts).
(I) Average firing frequency of the neuron in (H) during the initial rest, pre-locomotion, locomotion, post-locomotion, and subsequent rest periods.
(J) Spike frequency-treadmill velocity correlation (purple) versus the correlation after shuffling (orange, mean ± 2 SD).
(K) Peak correlation versus *Z* score for the sample population.
(L) The spiking rate of the neuron in (H) varied inconsistently over several cycles of velocity change (a, b, and c in H are color coded).
(M and N) Frequency (M) and *Z* score (N) population data for type 2 neurons in Q175 mice.
*$p < 0.05$; ns, not significant.

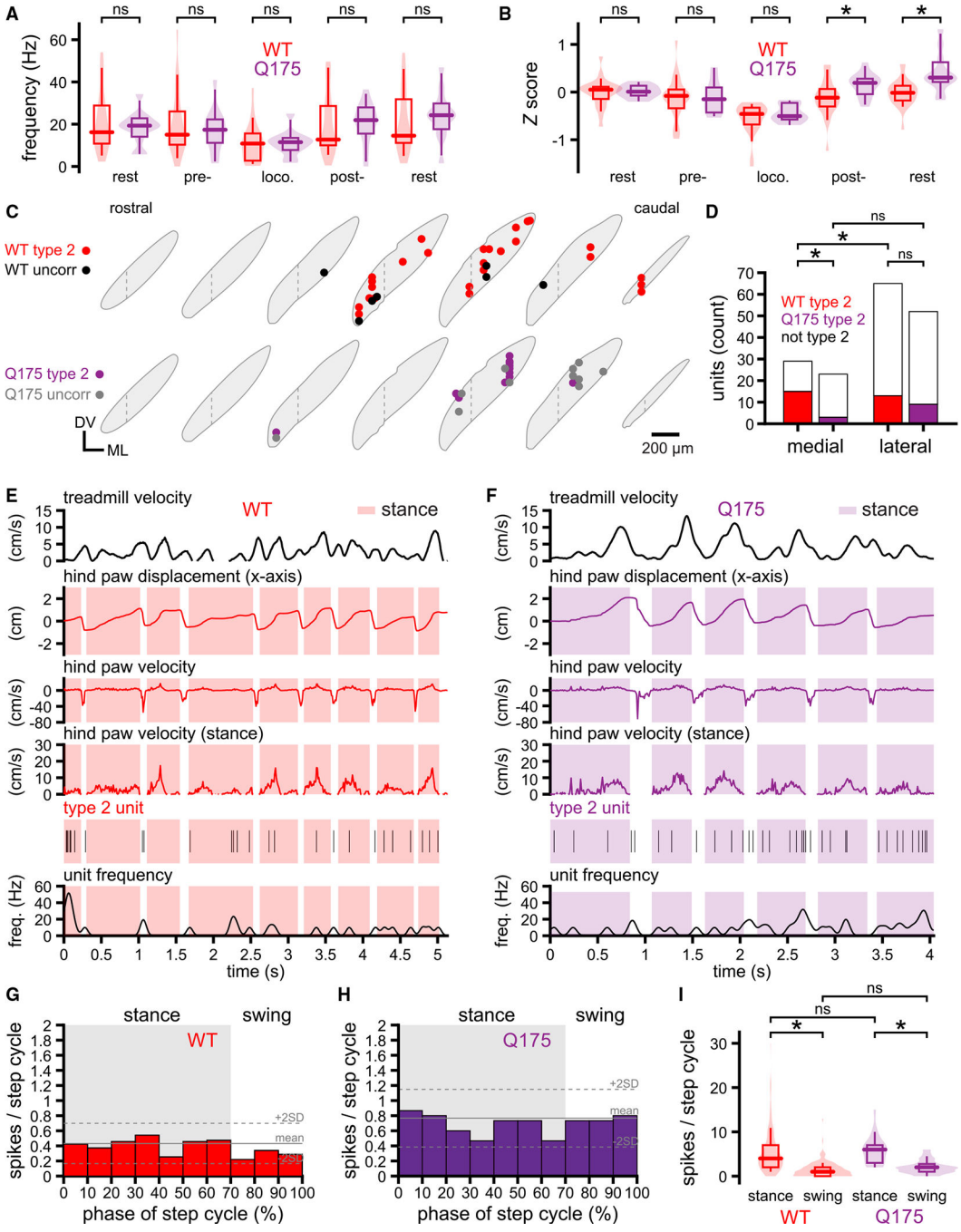

Figure 6. The frequencies and patterns of resting and locomotion-associated type 2 STN neuron activity are similar in WT and Q175 HD mice

(A and B) Population data. The frequencies (A) and *Z* scores (B) of resting and locomotion-associated type 2 STN activity were similar in WT and Q175 mice.

(C and D) Distribution of recorded type 2 STN neurons in WT and Q175 mice. The boundary between the medial third and lateral two-thirds of the STN is denoted by a dashed line. Type 2 units were located throughout the caudal half of the STN in WT and Q175 mice. Type 2 units were (1) more abundant in the medial than the lateral STN of WT mice and

(2) more abundant in the medial STN of WT mice than the medial STN of Q175 mice. The distribution of units whose activity was uncorrelated with locomotion is also illustrated (C). (E–I) Type 2 STN neurons in WT and Q175 mice exhibited firing that was unrelated to the phase of the locomotor cycle (E–H, representative examples; I, population data). (I) The number of spikes per locomotor cycle was similar in WT and Q175 mice.*$p < 0.05$; ns, not significant.

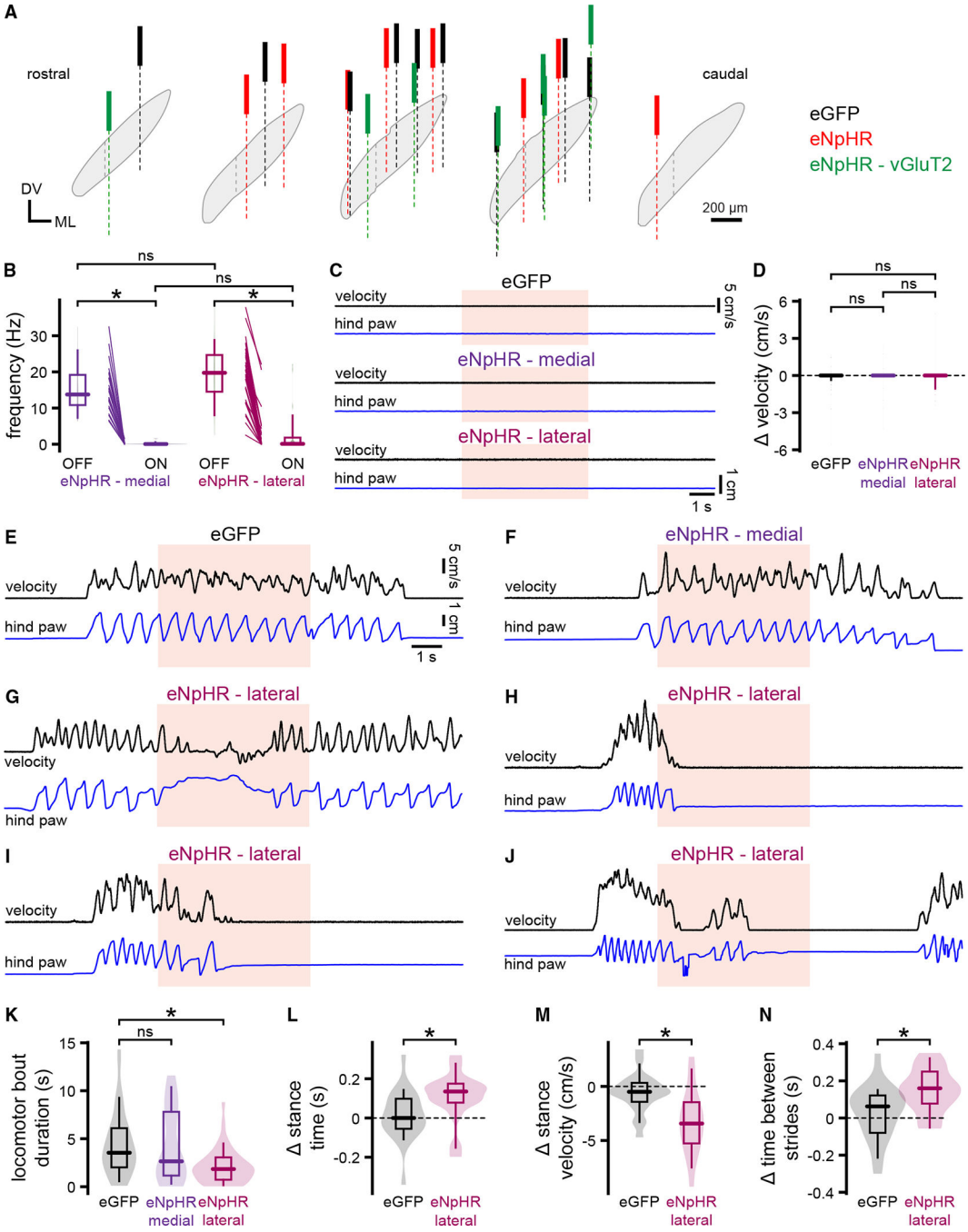

Figure 7. Optogenetic inhibition of movement-related STN activity dysregulates locomotion

(A) Positions of the fiberoptics used to deliver 633-nm light to the STN in control eGFP-expressing WT mice (black), eNpHR3.0-eYFP-expressing WT mice (red), and eNpHR3.0-eYFP-expressing vGluT2-Cre mice (green). The boundary between the medial third and lateral two-thirds of the STN is denoted by a dashed line. The histological section used to determine the location of the most lateral fiberoptic in the 2nd panel from the left is illustrated in Figure S6B.

(B) Impact of stimulating eNpHR3.0-eYFP in the medial third or lateral two-thirds of the STN on neuronal activity.

(C and D) Effects of 633-nm STN light delivery (orange) for 5-s on eGFP- or eNpHR3.0-eYFP-expressing resting mice on treadmill velocity and hindpaw kinematics (C, representative examples; upper trace, treadmill velocity; lower trace, hindpaw x axis displacement; D, population data).

(E–J) Representative examples of the effects of 633-nm light delivery (orange) for 5-s on eGFP- or eNpHR3.0-eYFP-expressing mice during locomotion (upper traces, treadmill velocity; lower traces, hindpaw x axis displacement). Relative to the effects of light delivery in eGFP-expressing control mice (E), optogenetic inhibition of the medial STN had no effect on locomotion (F). In contrast, optogenetic inhibition of the lateral STN dysregulated, slowed, and more rapidly terminated locomotion compared to locomotor bouts in control mice (G–J).

(K–N) Population data. Compared to the effects of 633 nm light in eGFP-expressing control mice, optogenetic inhibition of the lateral STN reduced the duration of self-initiated locomotor bouts (K). In contrast, optogenetic inhibition of the medial STN had no effect on bout duration (K). Optogenetic inhibition of the lateral STN also increased the duration (L) and reduced the velocity (M) of the contralateral hindlimb's locomotor cycle, and increased the time between strides (N). *$p < 0.05$; ns, not significant.

KEY RESOURCES TABLE

REAGENT or RESOURCE	SOURCE	IDENTIFIER
Antibodies		
Anti-Iba1, Rabbit antibody	FUJIFILM Wako Pure Chemical Corporation	Cat#019–19741; RRID:AB_839504
Anti-NeuN, Mouse antibody	Abcam	Cat# ab104224; RRID:AB_10711040
Anti-Parvalbumin, Guinea pig antibody	Synaptic Systems	Cat#195 004; RRID:AB_2156476
Alexa Fluor 405, Donkey anti-Mouse IgG (H + L)	Thermo Fisher Scientific	Cat#A48257; RRID:AB_2884884
Alexa Fluor 594-AffiniPure Donkey Anti-Guinea Pig IgG (H + L)	Jackson ImmunoResearch Laboratories, Inc.	Cat#706-585-148; RRID:AB_2340474
Alexa Fluor 488-AffiniPure Donkey Anti-Mouse IgG (H + L)	Jackson ImmunoResearch Laboratories, Inc.	Cat#715-545-150; RRID:AB_2340846
Alexa Fluor 594-AffiniPure Donkey Anti-Mouse IgG (H + L)	Jackson ImmunoResearch Laboratories, Inc.	Cat#715-585-150; RRID:AB_2340854
Alexa Fluor 647-AffiniPure Donkey Anti-Mouse IgG (H + L)	Jackson ImmunoResearch Laboratories, Inc.	Cat#715-605-151; RRID:AB_2340863
Alexa Fluor 488-AffiniPure Donkey Anti-Rabbit IgG (H + L)	Jackson ImmunoResearch Laboratories, Inc.	Cat#711-545-152; RRID:AB_2313584
Alexa Fluor 594 AffiniPure Donkey Anti-Rabbit IgG (H + L)	Jackson ImmunoResearch Laboratories, Inc.	Cat#711-585-152; RRID:AB_2340621
Alexa Fluor 647-AffiniPure Donkey Anti-Rabbit IgG (H + L)	Jackson ImmunoResearch Laboratories, Inc.	Cat#711-605-152; RRID: AB_2492288
Bacterial and virus strains		
AAV9-CaMKIIa-eNpHR3.0-eYFP	pAAV-CaMKIIa-eNpHR 3.0-EYFP was a gift from Karl Deisseroth	Addgene viral prep #26971-AAV9
AAV9-Ef1a-DIO-eNpHR3.0-eYFP	(Gradinaru et al.)[93]	Addgene viral prep #26966-AAV9
AAV9.EF1a.DIO.hChR2(H134R)-eYFP.WPRE.hGH	pAAV-EF1a-double floxed-hChR2(H134R)-EYFP-WPRE-HGHpA was a gift from Karl Deisseroth	Addgene viral prep #20298-AAV9
AAV9-hSyn-eGFP	pAAV-hSyn-EGFP was a gift from Bryan Roth	Addgene viral prep #50465-AAV9
Chemicals, peptides, and recombinant proteins		
DiI red	Thermo Fisher Scientific	Cat#D282
Experimental models: Organisms/strains		
Mouse: C57BL/6J	The Jackson Laboratory	RRID:IMSR_JAX:000664
Mouse: B6.129S1-Htt^{tm11Mfc}/190ChdiJ	The Jackson Laboratory	RRID:IMSR_JAX:029928
Mouse: B6J.129S6(FVB)-Slc17a6$^{tm2(cre)Low}$/MwarJ	The Jackson Laboratory	RRID:IMSR_JAX:028863
Mouse: B6.Cg-Pvalb$^{tm11(cre)Aibs}$/J	The Jackson Laboratory	RRID:IMSR_JAX:012358
Software and algorithms		
DeepLabCut	(Mathis et al.)[64]	RRID:SCR_021391
Fiji	(Schindelin et al.)[94]	https://imagej.net/software/fiji/; RRID:SCR_003070

REAGENT or RESOURCE	SOURCE	IDENTIFIER
Illustrator	Adobe	http://www.adobe.com/products/illustrator.html; RRID:SCR_010279
Mathematica	Wolfram Mathematica	https://www.wolfram.com/mathematica/; RRID:SCR_014448
MATLAB	MathWorks	http://www.mathworks.com/products/matlab/; RRID:SCR_001622
NeuroExplorer	Nex Technologies	http://www.neuroexplorer.com/; RRID:SCR_001818
NeuroInfo	MBF Bioscience	https://www.mbfbioscience.com/neuroinfo; RRID:SCR_017346
Plexon Offline Sorter software	Plexon, Inc.	http://www.plexon.com/products/offline-sorter; RRID:SCR_000012
Prism	GraphPad	http://www.graphpad.com/; RRID:SCR_002798
R Project for Statistical Computing	(Dessau and Pipper)[95]	http://www.r-project.org/; RRID:SCR_001905